ENHANCEMENT OF THERMOELECTRIC PROPERTIES FOR DOPED SKUTTERUDITES BASED ON $CoSb_3$ THROUGH BALL MILLING PARAMETRIC OPTIMIZATION

MD OVIK RAIHAN

FACULTY OF ENGINEERING
UNIVERSITY OF MALAYA
KUALA LUMPUR

2018

ENHANCEMENT OF THERMOELECTRIC PROPERTIES FOR DOPED SKUTTERUDITES BASED ON $CoSb_3$ THROUGH BALL MILLING PARAMETRIC OPTIMIZATION

MD OVIK RAIHAN

THESIS SUBMITTED IN FULFILMENT OF THE REQUIREMENTS FOR THE DEGREE OF MASTER OF ENGINEERING SCIENCE

FACULTY OF ENGINEERING
UNIVERSITY OF MALAYA
KUALA LUMPUR

2018

UNIVERSITY OF MALAYA

ORIGINAL LITERARY WORK DECLARATION

Name of Candidate: **MD Ovik Raihan**

Matric No: KGA140040

Name of Degree: Master of Engineering Science

Title of Project Paper/Research Report/Dissertation/Thesis ("this Work"): **Enhancement of Thermoelectric Properties for Doped Skutterudites Based on $CoSb_3$ through Ball Milling Parametric Optimization**

Field of Study: **Engineering Materials**

I do solemnly and sincerely declare that:

(1) I am the sole author/writer of this Work;
(2) This Work is original;
(3) Any use of any work in which copyright exists was done by way of fair dealing and for permitted purposes and any excerpt or extract from, or reference to or reproduction of any copyright work has been disclosed expressly and sufficiently and the title of the Work and its authorship have been acknowledged in this Work;
(4) I do not have any actual knowledge nor do I ought reasonably to know that the making of this work constitutes an infringement of any copyright work;
(5) I hereby assign all and every rights in the copyright to this Work to the University of Malaya ("UM"), who henceforth shall be owner of the copyright in this Work and that any reproduction or use in any form or by any means whatsoever is prohibited without the written consent of UM having been first had and obtained;
(6) I am fully aware that if in the course of making this Work I have infringed any copyright whether intentionally or otherwise, I may be subject to legal action or any other action as may be determined by UM.

Candidate's Signature Date:

Subscribed and solemnly declared before,

Witness's Signature Date:

Name:

Designation:

UNIVERSITI MALAYA

PERAKUAN KEASLIAN PENULISAN

Nama: **MD Ovik Raihan**

No. Matrik: KGA140040

Nama Ijazah: Ijazah Sarjana Kejuruteraan Sains

Tajuk Kertas Projek/Laporan Penyelidikan/Disertasi/Tesis ("Hasil Kerja ini"):

Enhancement of Thermoelectric Properties for Doped Skutterudites Based on $CoSb_3$ through Ball Milling Parametric Optimization

Bidang Penyelidikan: **Engineering Materials**

Saya dengan sesungguhnya dan sebenarnya mengaku bahawa:

(1) Saya adalah satu-satunya pengarang/penulis Hasil Kerja ini;
(2) Hasil Kerja ini adalah asli;
(3) Apa-apa penggunaan mana-mana hasil kerja yang mengandungi hakcipta telah dilakukan secara urusan yang wajar dan bagi maksud yang dibenarkan dan apa-apa petikan, ekstrak, rujukan atau pengeluaran semula daripada atau kepada mana-mana hasil kerja yang mengandungi hakcipta telah dinyatakan dengan sejelasnya dan secukupnya dan satu pengiktirafan tajuk hasil kerja tersebut dan pengarang/penulisnya telah dilakukan di dalam Hasil Kerja ini;
(4) Saya tidak mempunyai apa-apa pengetahuan sebenar atau patut semunasabahnya tahu bahawa penghasilan Hasil Kerja ini melanggar suatu hakcipta hasil kerja yang lain;
(5) Saya dengan ini menyerahkan kesemua dan tiap-tiap hak yang terkandung di dalam hakcipta Hasil Kerja ini kepada Universiti Malaya ("UM") yang seterusnya mula dari sekarang adalah tuan punya kepada hakcipta di dalam Hasil Kerja ini dan apa-apa pengeluaran semula atau penggunaan dalam apa jua bentuk atau dengan apa juga cara sekalipun adalah dilarang tanpa terlebih dahulu mendapat kebenaran bertulis dari UM;
(6) Saya sedar sepenuhnya sekiranya dalam masa penghasilan Hasil Kerja ini saya telah melanggar suatu hakcipta hasil kerja yang lain sama ada dengan niat atau sebaliknya, saya boleh dikenakan tindakan undang-undang atau apa-apa tindakan lain sebagaimana yang diputuskan oleh UM.

Tandatangan Calon Tarikh:

Diperbuat dan sesungguhnya diakui di hadapan,

Tandatangan Saksi Tarikh:

Nama:

Jawatan:

ENHANCEMENT OF THERMOELECTRIC PROPERTIES FOR DOPED SKUTTERUDITES BASED ON $CoSb_3$ THROUGH BALL MILLING PARAMETRIC OPTIMIZATION

ABSTRACT

In search for green energy harvesting materials, thermoelectric technology has been identified as a promising technology to generate electricity from waste heat through the presence of a temperature gradient. Skutterudite a viable candidate for high performance thermoelectric material given its advantages of modifying its structure such as doping, filling, substitution in its cage structure to achieve high performance; making its one of the sophisticated member of the thermoelectric application. In this work a new composition of Bi doped and Fe substituted Co_3Sb_{12} system was successfully synthesized by two step process namely ball milling and spark plasma sintering. The ball milling process produce nanostructures. Which are expected to give superior TE properties through reduction in thermal conductivity. Three different ball milling time were investigated: 10h, 15h, 20 h and their correlation to the thermoelectric properties studied in this thesis. Introduction of the Co and Bi with heat treatment resulted in a successful formation of $Bi_{0.6}FeCo_3Sb_{12}$ skutterudite. Which is expected to give better thermoelectric performance through substitution of Co with Fe and the Bi doping. The phase structure and morphology of the bulk samples were examined by X-ray diffraction (XRD) and scanning electron microscopy integrated energy-dispersive X-ray spectroscopy analysis (SEM-EDS), respectively. . Rietveld analysis of its XRD spectra indicated that the Bi doping on the Co_4Sb_{12} based skutterudite succeeded in partially filling the voids of the skutterudite, whilst the Fe doping partially substituted the Co sites in the lattice. The thermoelectric properties of the Bi filled and Fe substituted bulk samples were measured in a temperature range of 373 K to 673 K. Evidently all of the Bi doped and Fe substituted samples showed a dominant phase of $CoSb_3$ skutterudite. Comparative study among the

Bi filled, Fe substituted samples were done. The ball milling times was correlated to the resulting microstructure, and ultimately, its thermoelectric performance. It was found that the moderate ball milling times (at 15 hours) resulted in the best electrical conductivity of 122K $\Omega^{-1}m^{-1}$ at 373 K, given the homogenous distribution of particles. A Maximum ZT value was observed 0.17 for 10 h ball milled sample at 673 K, whilst almost the same value was achieved for the 15 h ball milled sample , i.e ZT =0.169 at 673 K. This work provides a pathway for improvement of the electrical conductivity and decreasing the thermal conductivity, and is thus a useful strategy for future design of skutterudite materials for thermoelectrics. The analysis of the effect of the ball milling conditions on the thermoelectric performance of this formulations also gives insight to the optimal conditions which may yield a good microstructure, and hence good thermoelectric performance. It has been shown that moderate milling times will provide a well distributed sample which is conducive for good electrical conductivity and low thermal conductivity. This work also demonstrated that milling time is able to affect the final composition of the skutterudite in terms of the amount of Bi filling, despite using the same nominal composition for all three samples.

Keywords: Ball milling, Parametric Optimization, SPS, Thermoelectric Properties, Microstructure Analysis

PENAMBAHBAIKAN SIFAT-SIFAT TERMOELEKTRIK BAGI SKUTTERUDITES TERISI BERASASKAN $CoSb_3$ MELALUI CARA PENGGILINGAN BOLA DENGAN PENGOPTIMUMAN PARAMETER

ABSTRAK

Pencarian bahan penuaian tenaga hijau, teknologi termoelektrik telah dikenalpasti sebagai teknologi yang menjanjikan untuk menjana elektrik dari haba buangan melalui kehadiran perubahan suhu. Skutterudite merupakan calon yang berdaya maju untuk bahan termoelektik yang berprestasi tinggi kerana kelebihannya mengubah strukturnya melalui doping, pengisian, penggantian struktur sangkar bagi mencapai prestasi tinggi; ianya akan menjadikan salah satu daripada bahan unggul dalam aplikasi termoelektrik itu. Dalam kajian ini, satu komposisi baru Bi doped dan Fe menggantikan dalam sistem Co3Sb12 telah berjaya disintesis oleh dua langkah proses iaitu pengilangan bola dan percikan plasma sintering. Proses pengilangan bola menghasilkan struktur nano yang dijangka akan menjadikan sifat-sifat termoelekrik yang lebih unggul melalui pengurangan kekonduksian terma. Dalam tesis ini, tiga masa pengilangan bola yang berbeza telah diselidiki: 10 h, 15 h, 20 h dan korelasinya terhadap sifat-sifat termoelektrik Penambahan Co dan Bi dengan rawatan haba telah menghasilkan pembentukan $Bi_{0.6}FeCo_3Sb_{12}$ skutterudite. Hal ini diharapkan dapat memberikan prestasi termoelektrik yang lebih baik melalui penggantian Co dengan Fe dan doping Bi. Struktur fasa dan morfologi sampel pukal diteliti oleh X-ray difraksi (XRD) dan pengamatan mikroskop elektron mikroskopis sinar-dispersive analisis sinar-X (SEM-EDS). Rietveld analisis pektrum XRD menunjukkan bahawa doping Bi pada skutterudite berasaskan Co4Sb12 berjaya mengisi separa lompang skutterudite, sementara itu doping Fe separa menggantikan tapak Co dalam kisi. Sifat-sifat termoelektrik sampel yang diisi dengan Bi dan Fe yang diisikan telah diukur dalam julat suhu 373 K hingga 673 K. Jelas sekali semua sampel yang

digantikan dengan doping Bi dan Fe menunjukkan fasa dominan $CoSb_3$ skutterudite. Kajian perbandingan antara sampel yang telah diisi oleh Bi serta penggantian dengan Fe telah dilakukan. Masa pengilangan bola dikaitkan dengan struktur mikro yang dihasilkan, dan juga prestasi termoelektriknya. Hasilnya didapati bahawa masa penggilingan bola yang sederhana (pada masa 15 jam) menghasilkan kekonduksian elektrik yang terbaik dari 122 K Ω-1m-1 pada 373 K, berdasarkan pembahagian zarah homogen. Nilai maksimum ZT diperhatikan di 0.17 bagi sampel pada 10 jam penggilingan bola pada suhu 673 K, manakala nilai yang hampir sama dicapai bagi sampel pada 15 jam penggilingan bola, iaitu ZT = 0.169 pada suhu 673 K. Kajian ini menyediakan laluan untuk penambahbaikan elektrik kekonduksian dan mengurangkan kekonduksian terma, dan oleh itu strategi yang berguna untuk reka bentuk masa depan bahan-bahan skutterudite untuk termoelektrik. Analisis kesan pengilingan bola pada prestasi termoelektrik dalam formulasi ini juga memberikan informasi tentang parameter optimum yang mungkin menghasilkan struktur mikro yang baik, dan oleh itu prestasi termoelektrik yang baik. Kajian telah menunjukkan bahawa masa penggilingan sederhana akan menyediakan sampel yang homogen untuk kekonduksian elektrik yang baik dan kekonduksian terma yang rendah. Kerja-kerja ini juga menunjukkan bahawa masa penggilingan dapat mempengaruhi komposisi terakhir skutterudite dari segi jumlah pengisian Bi, walaupun menggunakan komposisi nominal yang sama untuk ketiga-tiga sampel.

Keywords: Ball milling, Parametric Optimization, SPS, Thermoelectric Properties, Microstructure Analysis

ACKNOWLEDGEMENTS

First and foremost, I would like to sincerely acknowledge my supervisor, namely, Assoc. Prof. Dr. Suhana Mohd Said for giving me the opportunity to pursue my master study under her supervision. Followed by the guidelines, invaluable suggestions, recommendations, enthusiasm, motivation, constructive criticism and support. Not only in educational sector she helped me to look at life in different ways, taught me lessons that is vital and crucial in every aspects of life. Overall I could only describe my experience with her in one word – priceless.

My immense gratitude to Prof. Dr. Kaoru Kimura for giving me the opportunity to work under him. His and the lab members' in-depth knowledge sharing, full access to his laboratory facilities helped for building the pathway to complete my research work at the University of Tokyo. It was a lifetime experience and I am forever thankful for this opportunity.

I would like to show my respect to Dr. Bui Duc Long for guiding me through my first phase of my study. His contribution means a lot and taught me valuable lessons. For his role I was able to visit and work in Tokyo University, Japan. Which is one of my best research experiences. I will never forget this. Thank you for believing in me.

It is impossible to thank enough to my mother Shahida Alam and father Ferdous Alam for everything they did and doing since my birth. Without them and their tireless efforts I would be nothing and everything that I am today would be unmanageable. They are the best.

Besides, I would like to especially thank Ms Noor Shafinie Surapandi for everything she had done for me. From simple thing to crucial matters she was like a one stop solution holder and the most reliable person to go for advice, help, and guidelines. Pursuing my

dream would have been be a lot harder without her contribution. I will be forever in debt for her time and selfless effort.

Moreover the contribution of Ms Fitriani and Mohamed Bashir Ali Bashir in my research has great impact. Thank you for your valuable time, discussions, support and knowledge sharing.

Last but not the least, my deepest gratitude to Md Asiqur Rahman and Robi Shankar Datta. Without them I might not even think to pursue my degree in Malaysia. They are the best people in my life since my school. Furthermore I cannot thank enough to Jahirul Islam Asif and Maruf Ahmed for being there in every good and worst situations in Malaysia. Ethar Y. Salih and Mohamed Hamid Elsheikh are the lab mates and friends I would love to have always by my side. Working with these great people is an experience. I will cherish this experience all the way of my life.

Finally, I would like to quote from legendary John Lennon – "Count your age by friends, not years. Count your life by smiles, not tears." Therefore I believe that, I am so lucky to have such great mentors, family, friends and colleagues. Thank you from the bottom of my heart for being there for me always. As a person I cannot expect more.

TABLE OF CONTENTS

LIST OF FIGURES

LIST OF TABLES

LIST OF SYMBOLS AND ABBREVIATIONS

TE	:	Thermoelectric
Z	:	Thermoelectric figure of merit
ZT	:	Dimensionless thermoelectric figure of merit
α	:	Seebeck coefficient
σ	:	Electrical conductivity
T	:	Temperature
k	:	Thermal conductivity
PF	:	Power Factor
ΔV	:	Voltage difference
ΔT	:	Temperature difference
K_e	:	Electrons transporting heat
K_l	:	Phonons transporting heat
L	:	Lorenz number
K_B	:	Boltzman constant
e	:	Electron charge
$PGEC$	:	Phonon glass electron crystal
ρ	:	Electrical resistivity
C_V	:	Specific heat
V_s	:	Speed of sound
n_e	:	Carrier concentration
μ	:	mobility
h	:	Plank's constant
SPS	:	Spark plasma sintering
TEG	:	Thermoelectric generator

MA	:	Mechanical alloying
XRD	:	X-ray diffraction
SEM	:	Scanning electron microscopy
FESEM	:	Field emission scanning electron microscopy
EDS	:	Energy-dispersive X-ray spectroscopy
PCA	:	Process control agent
HP	:	Hot press
HIP	:	Hot isostatic pressing
FRC	:	Fiber reinforced ceramic
MMC	:	Metal matrix composite
FGM	:	Functionally graded materials

CHAPTER 1: INTRODUCTION

1.1 Introduction

The world is suffering from one a problem in electricity supply with regards to increasing energy demands worldwide. Furthermore, environmental issues arising from fossil fuel burning from conventional energy combustion. These conventional heat engines are running approximately 30 – 40% efficiency and the rest of the energy is lost by waste heat (T. Wang, Zhang, Peng, & Shu, 2011). Burning of fossil fuels to meet the energy demand plays a major role to the emission of greenhouse gases, effecting directly to the planet's environment and causing climate changes, pollutions and eventually leading to global warming (Dmitriev & Zvyagin, 2010; Kalkan, Young, & Celiktas, 2012) These issues relating to environment and energy are amongst this century's biggest challenges.

To aid this huge problem for mankind, renewable energy seemingly the hope for this crisis. Amongst the renewable energy solutions harnessing solar, geothermal, wave, wind, thermoelectric, radio-isotope, hydro are some of the most popular and vastly used methods of renewable energy. Heat recovery form wasted heat into electricity employs thermoelectric devices are the leading technology. Themoelectric devices or materials are directly related to the phenomenon of the ability of such devices to directly convert thermal energy to electrical energy and vice versa. TE devices wide boundary of working range and the potential of nanostructure modification for better performance making it one of the ideal and potential devices for development of a scalable, effective, solid state renewable energy devices. TE devices' working temperature range can be as low as milliwatt range to megawatt applications (Keskar et al., 2012; Kishi et al., 1999). Making TE devices are prospective candidate for energy harvesting from industrial to domestic sector including transportation sector (Hmood, Kadhim, & Hassan, 2013; Tomeš et al., 2010)

A schematic diagram in Figure 1.1 shows how waste heat can be recovered as electricity to mitigate energy consumption as well as reducing carbon footprints, greenhouse gases emission, pollution etc. Based on a 20% thermoelectric generator (TEG) efficiency it can be possible to reduce 40 million tons of CO_2 emission to the environment annually (Kawamoto, 2009). Using the principles and properties of TEGs its application ranges from electricity generation from waste heat to refrigeration, from car exhaust to space missions.

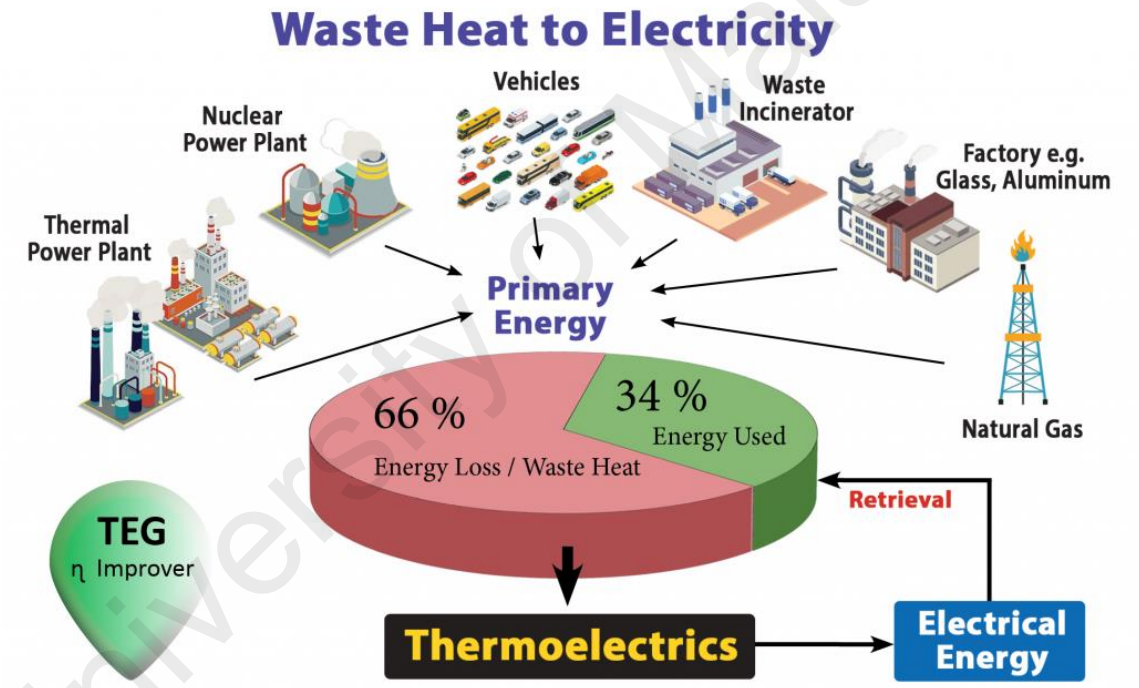

Figure 1.1: Schematic diagram of energy loss in everyday uses and potential of thermoelectricity to mitigate the huge loss. (Prometeon)

Considering the potential of thermoelectric devices intensive research is ongoing to develop thermoelectric materials for better efficiency, synthesis methods and to obtain low cost high performance materials for full scale industry production. To achieve these goals scientist and researchers developed some novel thermoelectric materials. For examples skutterudites, chalcogenides, silicides, clathrates, half-heuslers a few cases of

popular and widely investigated thermoelectric materials. Each of the materials are unique and has their own structural, thermoelectric, mechanical properties and different synthesis methods. For example filled skutterudite as thermoelectric material has low production cost, high mechanical strength, high oxidation resistance, thermal stability is good compare to the other thermoelectric materials, chemical stability and in mid temperature range of 300 - 800 K skutterudite materials show relatively high figure of merit (Truong, Kleinke, & Gascoin, 2014). One of the factors for significant improvement of thermoelectric materials is the introduction of nanostructures into thermoelectric materials to improve their performance, such as nanowires, quantum dots and superlattices. This was proposed in 1992 by Dresselhaus et al using Bi_2Te_3 in a quantum well structure which showed the potential of relatively higher value to quantum well structure over the bulk value. It also showed this kind of structure can certainly increase the overall figure of merit value of certain materials (Hicks & Dresselhaus, 1993)

The effect of nanotechnology has impressive effect on TE power generation. By using of nanotechnology it is evident that the improvement in the performance due to material synthesis is generating good results on the development of the TE devices. Which is so vast now a days that, it is now compared with the performance of the conventional materials. The performance of a TE material is determined by a dimensionless figure of merit (ZT), which is defined as

$$ZT = \frac{S^2 \sigma T}{k} \tag{1.1}$$

Here, S is the he Seebeck coefficient, σ is electrical conductivity, k is thermal conductivity and T is the absolute temperature. An efficient device mostly relies on the materials with high electrical conductivity (σ), high Seebeck coefficient (S) and low thermal conductivity (κ) for a steady solid-state thermoelectric energy conversion. With

the help of structural engineering it is already proven that the quantum and classical size effects has the ground for the tailoring of the electron and phonon transport properties in nanostructure. There were many techniques introduces such as quantum dots, quantum wells, superlattices to alteration of the density state of the electrons, band gaps, energy levels. It opens possibilities to the development of new thermoelectric materials. Besides the phonon scattering and interface reflections is being used to reduce thermal conductivity of the thermoelectric materials resulting improvement of this TE sector.

1.2 Thermoelectric devices and its applications

Thermoelectric devices are typically composed of pairs of heavily doped p-type and n-type semiconductors that are connected thermally in parallel and electrically in series. The devices contain no mechanically moving parts and thus are noise-free and very stable for long term operation. Since it has no moving parts and it will be low maintenance. Thermoelectric devices can be used for power generation and as a cooler.

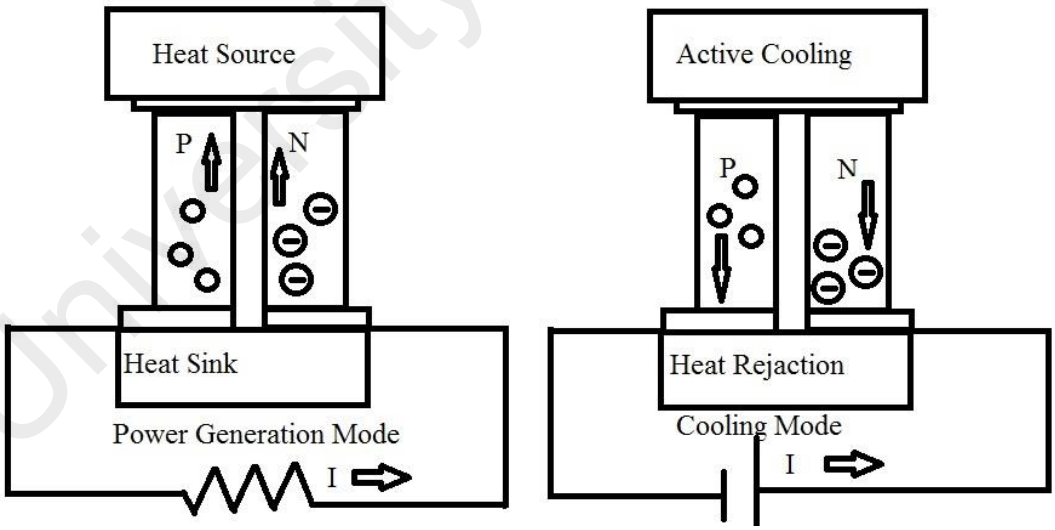

Figure 1.2: Simple schematic design to show how thermoelectric devices can be used for power generation (left) and cooling (right) (Nolas, Morelli, & Tritt, 1999).

It has been estimated that the majority of the world's power is generated by systems that typically operate at efficiencies of about 40% or less. Therefore there is an enormous need for thermoelectric systems that can 'salvage' the energy currently lost as heat to the environment (Rodgers, 2008). Uses of TE devices for the heat recovery is a popular way to recover the waste heat. The way to improve the sustainability of our electricity base is through the scavenging of waste heat with thermoelectric generators. Home heating, automotive exhaust, and industrial processes all generate waste heat that could be converted to electricity by using thermoelectrics. As thermoelectric generators are solid-state devices with no moving parts, they are silent, reliable and scalable, making them ideal for small, distributed power generation (Snyder & Toberer, 2008). The TE device can also be used for cooling application. As refrigerators, they are friendly to the environment due to the absence of CFC or any other refrigerant gas. Because of these advantages, the thermoelectric devices have found a large range of applications. The application of TE technology can be found in many areas in present days such as military, aerospace, instrument, biology, medicine and industrial or commercial products. The TE devices can be used as coolers, power generators, or thermal energy sensors. Small capacity TE coolers are being used extensively. But, due to the low efficiency, the application of the large capacity coolers and power generators are very limited. Recently a number of researches have been conducted by the researchers to apply this technology to recover waste from different systems. The increasing energy costs and environment protection regulations are compelled us to think about application of TE device.

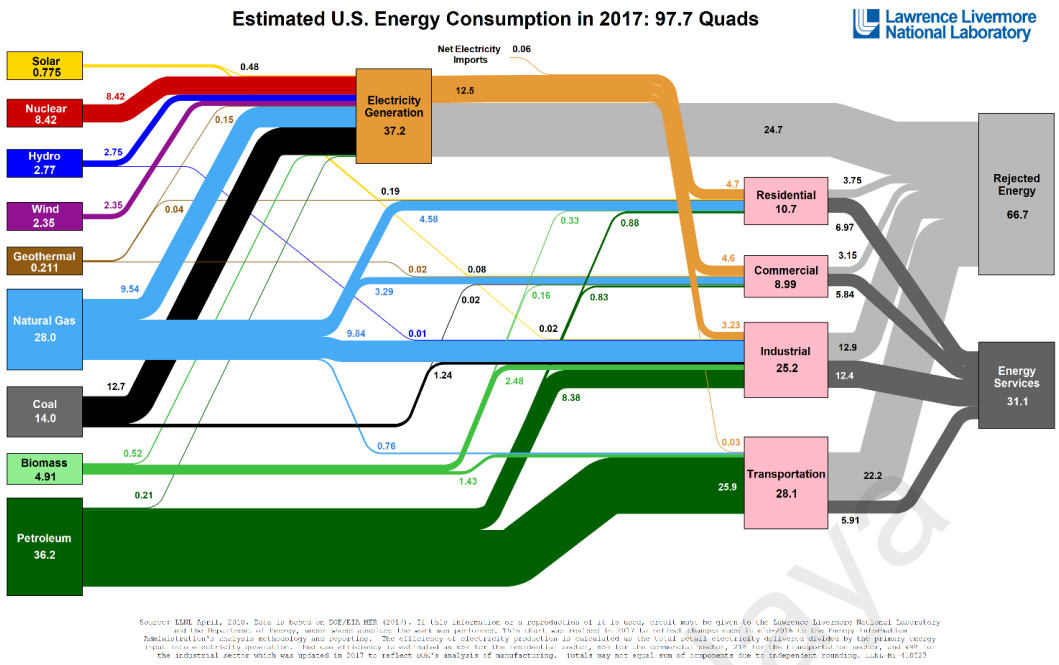

Figure 1.3: The energy loss in the form of energy loss in United States in 2017 (Lab, 2017).

In US alone approximately 66% of energy is lost in the form of wasted heat from 191 million vehicles. Which leads to the annual 36 TWh emission to the environment annually (Alam & Ramakrishna, 2013). Figure 1.3 shows the estimated energy consumption in the year of 2017 and the rejected energy. Considering the huge gap between the consumption and rejection amount of energy the world wide scenario needs aid to this major problem and thermoelectric devices can be the ideal candidate for potential solution.

1.3 Problem Statements

From the literature review above, we can see that skutterudite are an ideal and potential PGEC material has both the attraction for discovering new formulations and its properties. Also as a basic thermoelectric material researchers are working to enhance the thermoelectric properties and overall ZT. Numerous formulation and synthesis parameters along with multiple methods available, makes synthesis of skutterudites one of the complex TE materials, to optimize in a certain process parameter. Also these

separate process parameters has not been optimized due to different characteristics of the elements in the periodic table.

However, we can also see from the literature review that not many work has been done on identify optimal process parameter in producing high performance TE. Ball milling is one of the effective and popular synthesis process for TE materials. Due to its advantages of shortening milling time, storing energy into particle, temperature, grains sizes etc. For this study the synthesis of $Bi_{0.6}FeCo_3Sb_{12}$ through ball milling and spark plasma sintering will be conducted. As this formulations ball milling parameters yet not optimized, in this work we it be optimized and proposed. Investigation will be carried on the process parameters and its effect of the microstructure on this formulation. Along with optimization of the ball milling process parameters, study will be conducted to enhance the thermoelectric properties such as electrical conductivity and overall ZT.

1.4 Objectives

The aim of this research is to synthesize and characterize novel skutterudite based - TE material for recovering waste heat at an intermediate temperature range. The specific objectives of this research are enlisted below;

- Synthesis of $Bi_{0.6}FeCo_3Sb_{12}$ skutterudites for high efficiency thermoelectric properties.
- Optimize the effect of ball milling parameters on the thermoelectric properties of $Bi_{0.6}FeCo_3Sb_{12}$.
- Investigate the effects of the particle size and filling level of Bi after optimization on thermoelectric properties of $Bi_{0.6}FeCo_3Sb_{12}$.

CHAPTER 2: LITERATURE REVIEW

Thermoelectric materials with their properties lead to extraordinary potentials in the energy sector. Because there are many types of TE materials present and from material synthesis to device production the process parameters varies vastly. Formulations of these materials holds prospect and potential to achieve higher ZT along with development of certain thermoelectric parameters. There are several methods and synthesis methods available. Some of them are highlighted in the table no 1.1. Thus, extensive research is needed to find better process parameters, synthesis technique, formulations to achieve more efficient, high performance TE materials. For example, the study of "$Bi_xFeCoSb_3$" (x=0.6 has been used for this study) formulation has not been explored. Addition of Bi filler in the $FeCoSb_3$ skutterudite projects a probable outcome on high electrical conductivity due to its heavy atomic weight and electronic properties. Moreover optimization of the process parameter for this formulation will be proposed. Therefore due to the research gap on this formulation, it can be studied for process parameter optimization, microstructure, and increase of thermoelectric properties i.e electrical properties compared to $Cosb_3$ or $FeCoSb_3$. Synthesis of $Bi_{0.6}FeCoSb_{12}$ and its overall TE performance along with microstructure will be studied for this research. In the literature review below the process parameters and thermoelectric properties has been discussed extensively.

Table 2.1: Skutterudite compounds with their different synthesis process with their respective ZT.

Compound	ZT	**Article name**	**Process**	**References**
$Sm_{0.32}$ $Fe_{1.47}$ $Co_{2.53}$ Sb_{12}	0.63	Crystal Structures and Thermoelectric Properties of Sm-Filled Skutterudite Compounds $Sm_yFe_xCo_{4-x}Sb_{12}$	Melting-sps	(Taoxiang, Xinfeng, Wenjie, Yonggao, & Qingjie, 2007)
$Tl_{0.20}$ $(Co_{0.8}$ $Rh_{0.2})_4Sb_{12}$	0.58	Effects of Tl-filling into the voids and Rh substitution for Co on the thermoelectric properties of $CoSb_3$	Heating-quenching-annealing-hp	(Harnwunggmoung, Kurosaki, Ohishi, Muta, & Yamanaka, 2011)
$Ba_{0.18}$ $Ce_{0.05}$ $Co_4Sb_{12.02}$.	1.26	Enhanced thermoelectric performance of dual-element-filled skutterudites $Ba_xCe_yCo_4Sb_{12}$	Melting-quenching-annealing-sps	(Bai et al., 2009)
$Gd_{0.12}Co_4Sb_{12}$	0.52	Gadolinium filled$CoSb_3$: Highpressuresynthesis and thermoelectricproperties	CP-2 stage HPS-SPS	(Jianqing Yang et al., 2013)
$Yb_xIn_yCe_zCo_4Sb_{12}$	1.43	High thermoelectric performance of In,Yb,Cemultiple filled $CoSb_3$ based skutterudite compounds	Melting-annealing-SPS	(Ballikaya, Uzar, Yildirim, Salvador, & Uher, 2012)
$La_xFeCo_3Sb_{12}$	0.32	Preparation and thermoelectric properties of $La_xFeCo_3Sb_{12}$ skutterudites by mechanical alloying and hot pressing	BM-HP	(Bao, Yang, Peng, et al., 2006)
$In_zCo_4Sb_{12-y}Te_y$	0.55	Thermoelectric properties of $In_zCo_4Sb_{12-y}Te_y$ skutterudites	Encapsulated quartz tube inductionmelting. RF 40kW, 40kHz for 1 h	(Jung et al., 2007)

Compound	ZT	**Article name**	**Process**	**References**
Fe_3CoSb_{12} based skutterudite	$CoSb_3$ = 0.19 $LaFe_3CoSb_{12}$ = 0.43 $CeFe_3CoSb_{12}$ = 0.62 $La_{0.5}Ce_{0.5}Fe_3CoSb_{12}$ = 0.82	Thermoelectric properties of rare earths filled CoSb3 based nanostructure skutterudite	Hydro/solvo thermal method and HP	(Lu et al., 2010)
$Sm_xCo_4Sb_{12}$	$Sm_{0.1}Co_4Sb_{12}$ ZT=0.55	Thermoelectric properties of $SmxCo_4Sb_{12}$ prepared by high pressure and high temperature	Agate morter-spd machine	(Jiang et al., 2010)
$U_yFe_xCo_{4-x}Sb_{12}$	ZT = 0.55 for $U_{0.2}FeCo_3Sb_{12}$	Thermoelectric properties of uranium filled skutterudites $U_y(Fe_xCo_{4-x})Sb_{12}$	Arc melting-annealing-SPS	(Arita et al., 2005)
$In_xNd_yCo_4Sb_{12}$	0.11	Thermoelectricpropertiesindouble-filledskutterudites $In_xNd_yCo_4Sb_{12}$	Inductive melting method	(Tang, Zhang, Chen, Xu, & Wang, 2012)
p-$La_{0.7}Ba_{0.01}Ga_{0.1}Ti_{0.1}Fe_3Co_1Sb_{12}$	P type 0.75	Stability of Skutterudite Thermoelectric Materials	Annealing-water quenching – SPS	(Nie et al., 2014)
n-$Yb_{0.3}Ca_{0.1}Al_{0.1}Ga_{0.1}In_{0.1}Co_{3.75}Fe_{0.25}Sb_{12}$	N-type 1			
$La_xFe_4Sb_{12}$	0.41	Preparation and thermoelectric properties of La filled skutterudites by mechanical alloying and hot pressing	BM-HP	(Bao, Yang, Zhu, et al., 2006)
$Fe_xCo_{4-x}Sb_{12}$	0.3	Thermoelectric properties of Fe-doped $CoSb_3$ prepared by mechanical alloying and vacuum hot pressing	Attrition mill and HP	(Ur, Kwon, & Kim, 2007a)
$Yb_xFe_yCo_{4-y}Sb_{12}$	0.6	Thermoelectric properties of P-type Yb-filled skutterudite $Yb_xFe_yCo_{4-y}Sb_{12}$	Heat treatment-water quenching-BM-HP	(Zhou, Morelli, Zhou, Wang, & Uher, 2011)

2.1 Thermoelectric figure of merit

Thermoelectric figure of merit (ZT) is a measurement of the TE properties of materials which reflects the TE efficiency. It is used to determine the efficiency of the TE materials. The dimensionless figure of merit is proportional to the Seebeck coefficient squared, the temperature, and the electrical conductivity and inversely proportional to the thermal conductivity as shown in eq. no 1.1 Typical ranges in ZT are from zero, for poor TE materials, to 1.5 or more for high performance TE materials. Some examples of thin film TEs have been reported with ZT values reaching 2.5 or above (Venkatasubramanian, Siivola, Colpitts, & O'quinn, 2001), but these for the most part rely on thin film effects for their high efficiency thus limiting their general applicability to large-scale power generation problems. ZT depends on several material characteristics and does not have any theoretical upper limit, any ZT value above 1.5 for a bulk material is seen as a very encouraging result. There are some well-known systematic behaviors and trade-offs that affect the TE figures of merit of various materials. One important factor, although it does not appear directly in the ZT formula, is carrier concentration; one can readily see why TE research is concentrated in semiconductors instead of metal or insulators.

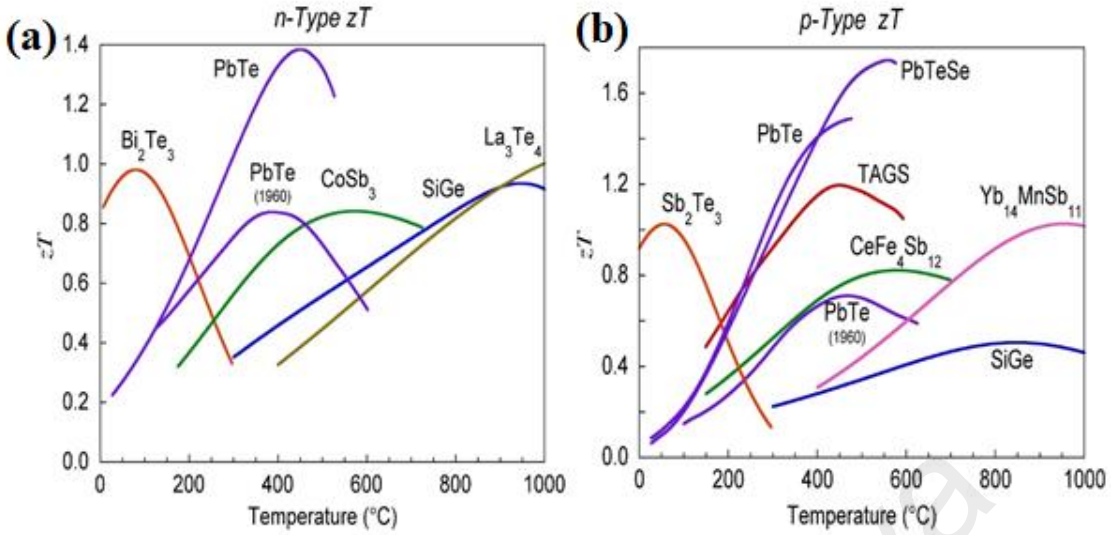

Figure 2.1: Dimensionless figure of merit, ZT as a function of temperature for (a) n-type and (b) p-type TE materials (Snyder & Toberer, 2008).

Although TE properties were first put to use with metal systems forming the basis of thermocouple operation, the high associated thermal conductivities make for poor TE materials. The various terms in the figure of merit, as plotted against carrier concentration, and therefore on an Insulator-Semiconductor-Metal axis, can be seen in Figure 2.1 (a) and (b).

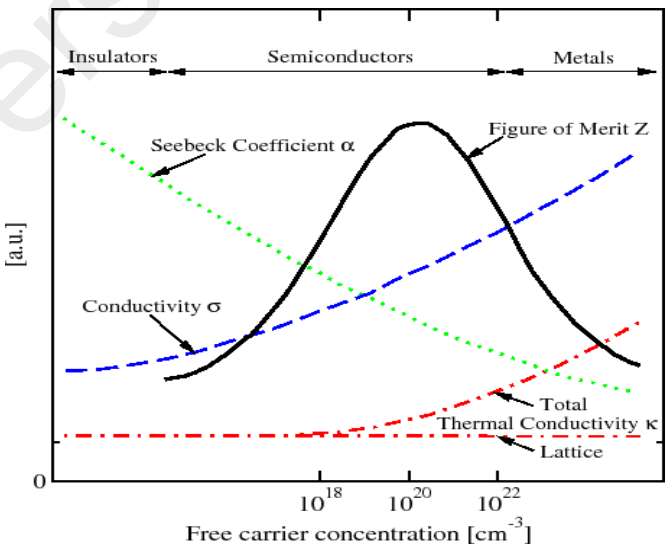

Figure 2.2: Carrier concentration, Seebeck coefficient, Conductivity, Figure of merit. (Dughaish, 2002).

Figure 2.2 shows carrier concentration dependence of individual TE properties. Metals and insulators are could not be used as good TE materials because of their unfavorable characteristic properties. Only semiconductor materials can be used as good TE material, which are having the carrier concentration around $10^{20}cm^{-3}$.

2.2 Thermoelectric material properties

2.2.1 Thermoelectric effect

All materials, to varying degrees, develop an electrical potential in response to an applied thermal gradient, this response is represented by the magnitude of the Seebeck coefficient. The Seebeck coefficient is a measure of proportionality between the thermal gradient on a material and resultant potential gradient generated in response to that thermal gradient. Charge carriers in a material have kinetic energy proportional to their temperature. Those charge carriers on the hot side of the thermal gradient will have higher kinetic energy than those on the cold side. These charge carriers will then move further between collisions and drift towards the cool side establishing an electrical potential difference in response to a thermal gradient. This electrical potential can develop either parallel or antiparallel to the thermal gradient, depending on the sign of the majority charge carriers in the material, as shown in Figure 2.3.

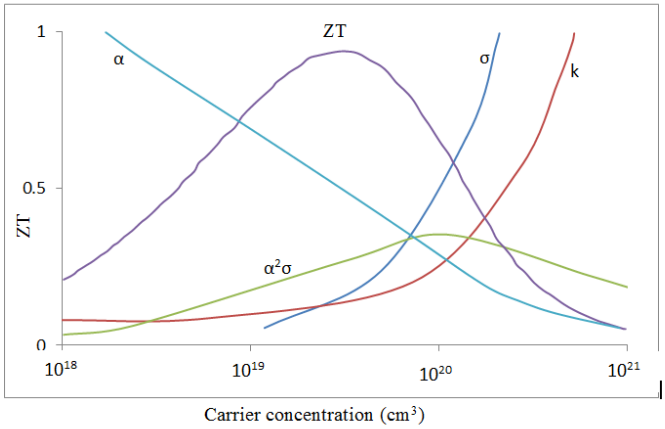

Figure 2.3: Optimizing ZT through carrier concentration tuning (Snyder & Toberer, 2008).

For increased efficiency of a TE device pair an n-type component (electron conductor) with a p-type component (hole conductor) in the TE circuit, as shown in Figure 2.4.

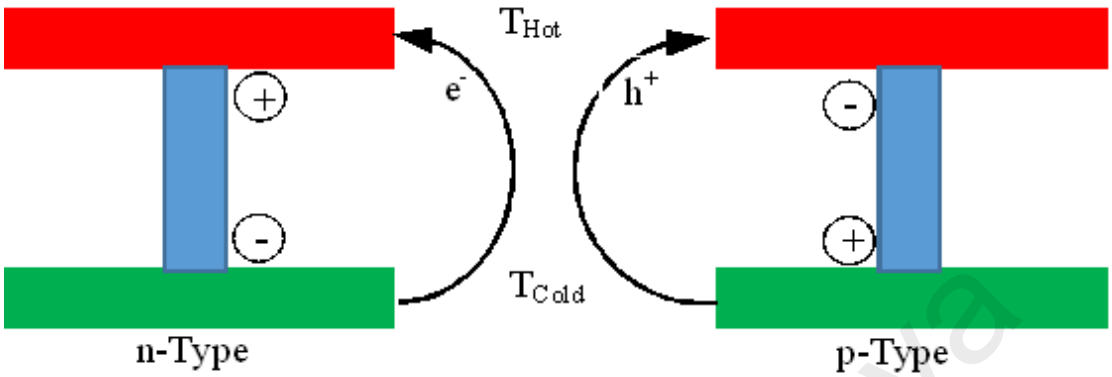

Figure 2.4: Schematic diagram of the response of n and p type materials to applied thermal gradient.

The external circuit, through which power is drawn out of the generator, connects the n and p legs, typically on the cold side of the generator, as shown in Figure 2.5.

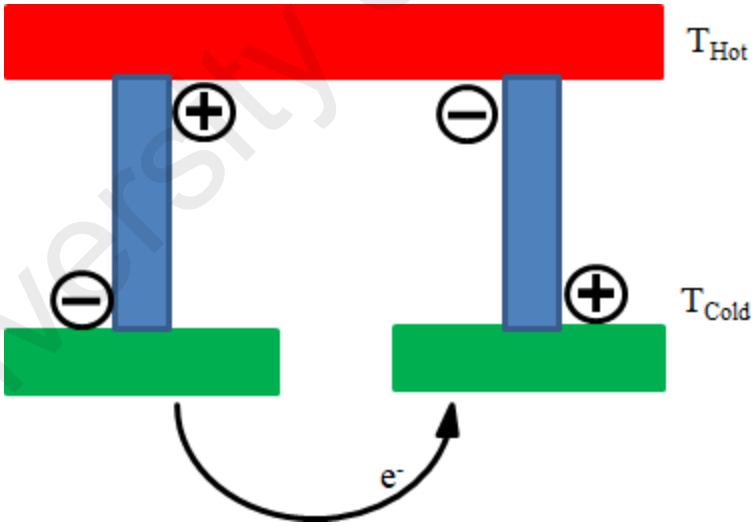

Figure 2.5: Schematic of typical unicouple configuration for a TEG.

To assure a strong current (large and steady), the seebeck coefficient of the materials must be high, and the resistivity and thermal conductivity must be low. Some of these attributes come at the cost of one another in most materials systems. If the electrical conductivity is too low, the charge carriers may not be free to carry much current, a poor design characteristic for a power generator. However the charge carriers tends to carry with it significant thermal conductivity since typical conductors have simple structures with low phonon scattering as well as thermal conduction via the majority charge carrier. If the thermal conductivity is too high, or the heat reservoirs are too small, the thermal gradient necessary to generate steady state power can collapse. These are some of the pertinent concerns in the search for new materials for TEG application.

2.2.2 Seebeck coefficient

The Seebeck coefficient (or so called thermoelectric power) of a material is the measure of the generated voltage between the two ends of a solid in response to a temperature difference across it. It has SI units of Volts per Kelvin (V/K), and more often is measured in microVolt per Kelvin (μV/K). The mathematical expression for the Seebeck coefficient is interrelated to material properties which is derived from a set of complex equations and is beyond the scope of our work. In general, the Seebeck coefficient, S can be expressed as,

$$S = \frac{\Delta V}{\Delta T} \tag{2.1}$$

So, Seebeck coefficient is the ratio of the generated voltage, ΔV and the temperature gradient between the hot side and the cold side, ΔT.

2.2.3 Thermal conductivity

Thermal conductivity describes the transport of energy – in the form of heat – through a body of mass as the result of a temperature gradient. The property that measures how easily heat is transmitted through a material. The thermal conductivity in TE materials is comprised of electronic contribution K_e and phonon (lattice) contribution K_l. K_e is directly related to the electrical conductivity through the Wiedemann-Franz law (Yan, 2010), which is expressed as follows:

$$K = K_e + K_i \tag{2.2}$$

$$K_e = L\sigma T \tag{2.3}$$

Where, L is the Lorenz number, which is 2.4×10^{-8} $J^2K^{-2}C^{-2}$ for metals. Total thermal conductivity is composed of two parts: electronic part and lattice/phonon part.

The electronic contribution to total thermal conductivity is proportional to the electrical conductivity, as indicated by the Wiedemann-Franz law as stated above. In heavily-doped semiconductors, the lorenz number is lower than that of metals (Yan, 2010). Lattice part of thermal conductivity gives us some independent control in improving ZT. According to the kinetic theory of gases, lattice thermal conductivity K_l in terms of the mean free - path of the phonons can be expressed as:

$$K_i = \frac{C_v V_s I}{3} \tag{2.4}$$

Where, C_V is the specific heat and V_s is the speed of sound. In our experiments, we limit the phonon mean - free path mainly by enhancing the boundary scattering through elemental substitution and ball milling.

2.2.4 Electrical conductivity

Electrical conductivity is the reciprocal of electrical resistivity, and measures a material's ability to conduct an electric current. It is the measure of a material's ability to accommodate the transport of an electric charge. Electrical conductivity (σ) quantifies charge carrier movement in response to an electric field; this expression describes the concentration (*n*e) and mobility (μ) of the charge carriers in a material:

$$\sigma = en_e\mu \tag{2.5}$$

Where, e is the fundamental charge of the electron/hole. The relationship between thermal and electrical conductivities in metals, bulk semiconductors is expressed by the Wiedemann-Franz law:

$$K = \sigma LT \tag{2.6}$$

This expression states that the ratio of conductivities is proportional to ambient temperature through the Lorenz number where, $L = л^2K_B^2/3e^2$ is a constant. Thus, it is difficult to vary one parameter without affecting the other. In bulk materials, it is challenging to further improve ZT due to the interrelated relationships among these three parameters. In other words, we cannot independently change individual property without affecting others.

2.3 Carrier concentration

The carrier concentration has a large effect on the electrical transport property. Figure 2.6 displaying the relation among the thermoelectric properties, figure of merit and carrier concentration.

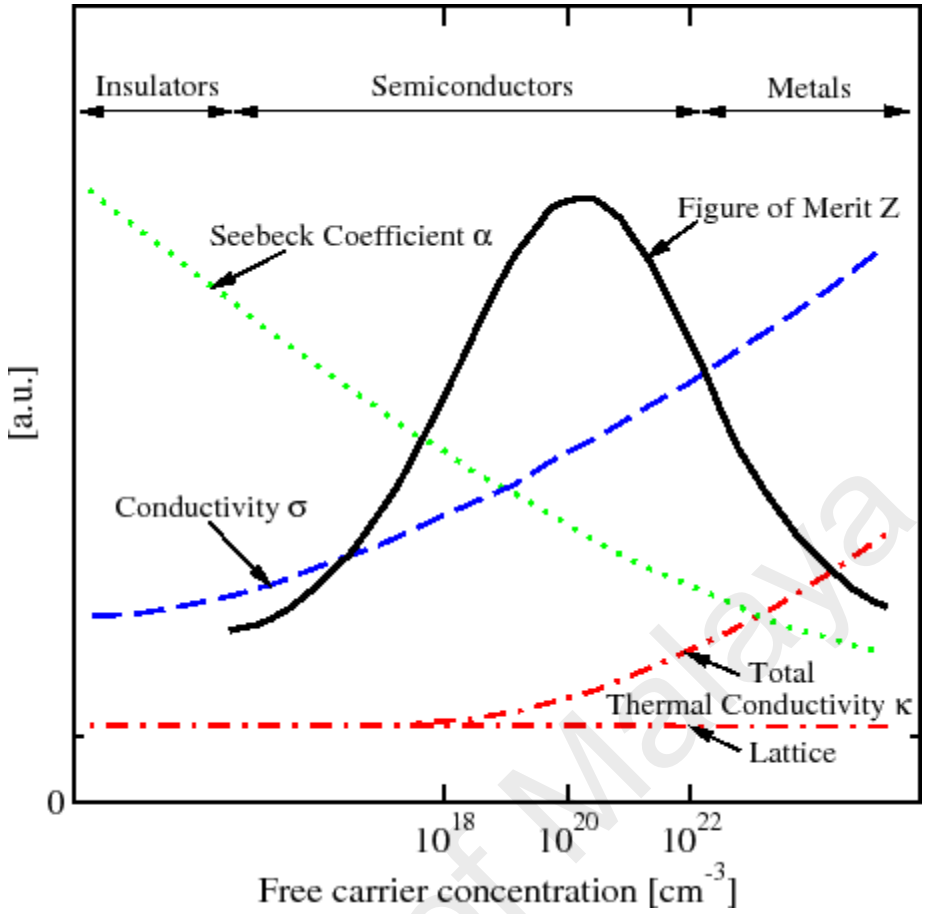

Figure 2.6: Carrier concentration.

This relations shows the affects and relationship on the dimensionless figure of merit (ZT) of the TE material. As mentioned in thermal conductivity part that the total thermal conductivity is depends on two part. The carrier carries the electrons. A high quality TE material must have a high electrical conductivity, low thermal conductivity and high thermopower. So to reduce thermal conductivity and improve electrical conductivity carrier concentration of TE material plays a vital role. The electrical conductivity formula is

$$\sigma = ne\mu \tag{2.7}$$

The electrical conductivity (σ) is related to the carrier concentration n through the carrier mobility μ.

For metals or degenerate semiconductors (parabolic band, energy-independent scattering approximation), the Seebeck coefficient is given by

$$\alpha = \frac{8л^2 K_B^2}{3eh^2} m \times T(\frac{л}{3n})^{2/3} \quad (2.8)$$

where m is mass of the carrier, e is charge of an electron, h and KB represents planks's constant and KB=Boltzmann constant respectively and T represent temperature. The effective mass of the charge carrier provides another conflict as large effective mass leads to low electrical conductivity, while low effective mass decreases Seebeck coefficient. High density-of-states effective mass is normally related to heavy carriers, which will move with slower velocities, resulting in smaller mobility and thus lower electrical conductivity. Basically high ZT is a trade-off between effective mass and mobility and can be found within a wide range of effective masses and mobilities.

2.4 Skutterudite

2.4.1 Crystal structure of skutterudite

There are various types of material in thermoelectric genre. But one of the most interesting, promising and yet to vastly discover is the Skutterudites. It has the basic qualities for good thermoelectric materials with high ZT like large unit cell, heavy constituent atom masses, low electronegativity differences between the constituent atoms and large carrier mobility (W. Liu, Yan, Chen, & Ren, 2012). In addition there are two "voids" per unit cell in the crystal structure of the skutterudite system.

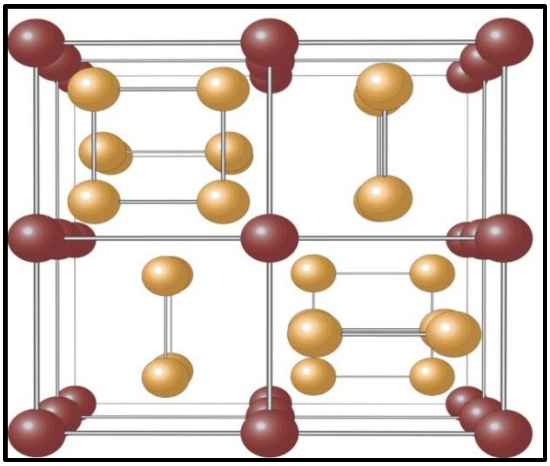

Figure 2.7: Schematic of skutterudite structure with void.

This specific group of materials has cubic structure (cubic Im3 (T_h^5) structure) and can be filled the void with "guest" atom (G. Chen et al., 2011). Introducing the guest atom in the void it is possible to tune up the thermal conductivity (Nolas, Slack, Morelli, Tritt, & Ehrlich, 1996). There are 9 binary semiconducting compounds in this group which can be represents with the formula unit AB_3 where A = Co, Rh and Ir are metal atoms. On the other hand B = P, As and Sb are the pnicogen atom. There are eight formula units per cubic cell and two of them are empty as shown in Figure 2.7. Skutterudites form covalent structures with low coordination numbers for the constituent atoms and so can incorporate atoms in the voids (G. Chen et al., 2011). When incorporated with "filler" atoms the skutterudite is called "filled skutterudites" and can be expressed as the general formula of $M_yA_4B_{12}$ (Schnelle et al., 2008). Here M represents the filler atom. Filler atom can be alkali, rare-earth, alkaline-earth, actinide metal or thallium. There are different degree of filling y is possible and y can be realized upto y=1 (Schnelle et al., 2008). When filled with a filler atom in the void of skutterudites; the atom starts to "rattle" and scatters the phonons, thus reducing the phonon propagation (G. Chen et al., 2011). How large is the void it can be measured by a formula. The radius r(B) of the B atom is taken to be one half of the average B-B separation. The void radius is taken as the distance d from the

center of the void to any of the twelve surrounding B atoms minus r(B) (G. Chen et al., 2011).

$$r(viod) = d - r(B) \tag{2.9}$$

Skutterudite systems have attracted a great attention from TE community due to their high Seebeck coefficient, excellent electrical transport properties and special lattice structure as shown in Figure 2.1. However, thermal conductivity of skutterudites is relatively high (>10 W/mK) which is contributed to the low ZT. Nanostructured skutterudites have shown a potential application at the temperature range of 500 - 900 K (Schnelle et al., 2008), (Wei, Zhang, & Zhang, 2014), (Zhao, Geng, & Teng, 2012), (K. Yang et al., 2009), (K. Liu, Dong, & Jiuxing, 2006), (Long Zhang & Sakamoto, 2013)

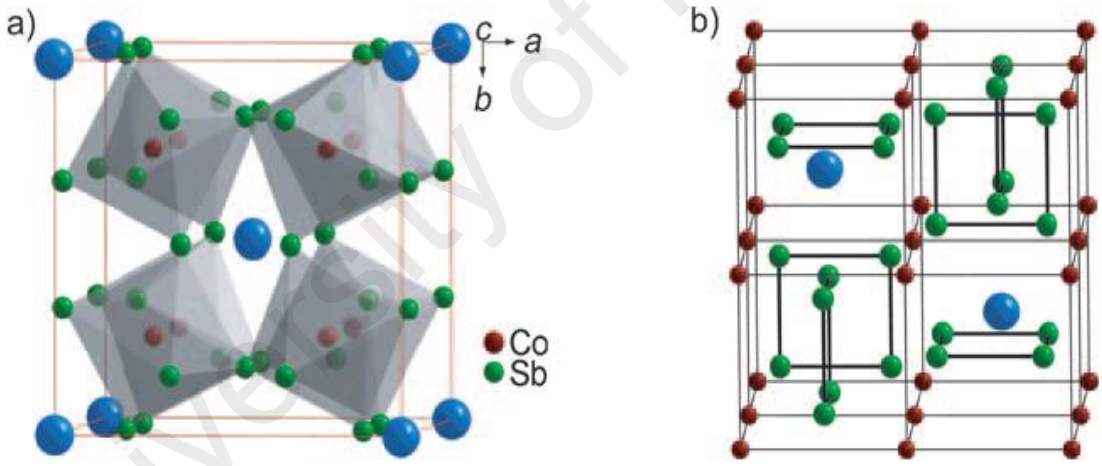

Figure 2.8: Simulation of the unfilled $CoSb_3$ skutterudite's two model structures (a & b) Co atoms and Sb atoms are shown by red and blue sphere, respectively and the blue ones are for showing the void cages (Sootsman, Chung, & Kanatzidis, 2009).

Figure 2.8 showing the simulated atom placement and void for $CoSb_3$ skutterudite. The blue spheres in the pictures can be filled or replaced by the other atoms. Which if successfully done can be lead to the potential PGEC behavior based filled skutterudite with high TE performance.

2.4.2 Recent development of skutterudites

Nanostructured skutterudites can be designed in such a way that disconnects the bonding between the electrical and thermal conductivity in order to increase the electrical conductivity without or less effect on the thermal conductivity (Rubi, Gowthaman, & Renganathan). This is one of the major breakthroughs for the PGEC material like behavior. Ball milling (BM) is one of the popular ways to reducing the grain size for nanostructuring. L.Zhang et al. (L Zhang et al., 2010), (L Zhang et al., 2009), G Rogl et al. (Rogl, Grytsiv, Bauer, Rogl, & Zehetbauer, 2010) produced their $E_yFe_4Sb_{12}$ and $E_yFe_3CoSb_{12}$ (where E= Ca, DD and Ba) skutterudites's powder samples with the grain size bellow 100-200 nm which was prepared by melting in quartz tubes, and following by annealing, ball milling and hot pressing. These methods improves the figure of merit ZT for their samples in different temperature range. There are actually several methods and researchers are trying to improve the TE properties applying several methods in order to enhance the figure of merit.

Arc melting, BM-SPS, SPS, Hot pressing are some of the popular synthesis methods for skutterudite. The synthesis through these methods has advantages over the conventional long time annealing/sintering methods. All of the stated methods have the advantage of rapid heating thus reducing the time and energy consumption. Arc melting uses arc current to melt the powders placed in the arc furnace in stoichiometric ratio. BM-SPS method is one of the most popular methods due to its advantages of mechanical alloying through ball milling and ability to reduce powders from micro to nano size. Then spark plasma sintering uses rapid heating using DC current in the furnace applying pressure at the same time. Hot pressing can also apply the pressure and heat at the same time. However hot pressing does not use DC current to sinter, thus it is not as rapid as SPS. Rapid heating helps to minimize the grain growth of the materials during the sintering process. These processes also comes with the facility to synthesize materials in

vacuum or noble gas environment. The implication and combination of these methods gives enhanced results in thermoelectric performances.

For example (L. Zhang et al., 2009) sample's prepared by BM was able to display a ZT of 0.52 at 740K. Which was reported 20% increment than the previous approach. It was stated that the reduced grain size helped to induce nano sized oxide composites resulting to lower the lattice thermal conductivity which helps to improve the ZT. Other nanostructured approaches also showing significant improvement of ZT for high temperature applications. $(GaSb)_{0.2}$-$Yb_{0.26}Co_4Sb_{12}$, $MCoSb_3$ (M=In,Ce) nanocomposite is showing a ZT value of ~1.45 at 850 K (X. Wang et al., 2008) and ZT ~ 1.43 at 800 K (Hochbaum et al., 2008) (Li, Liu, Zhao, & Zhou, 2010), respectively. $Ba_{0.08}La_{0.05}Yb_{0.04}Co_4Sb_{12}$ has the high ZT value of ~ 1.7 at 850 K (Shi et al., 2011). In the most recent and highest ZT value ~ 2.0 is reported of $Sr_{0.09}Ba_{0.11}Yb_{0.05}Co_4Sb_{12}$ skutterudite 835 K (Rogl et al., 2014). In this high ZT approach consecutive melting-annealing-melting was done. The powder was ground by mortar, and subsequently hot pressed. Ball milling was repeated to create nansized grains. Optimisation of process parameters to identify the ideal nanostructures for thermoelectrics is still a rich area to be researched, and this project focuses on the variation on ball milling parameters and its impact on crystallographic, microstructural and thermoelectric properties.

2.5 Mechanical alloying

Mechanical alloying (MA) is a materials-processing method that can produce homogeneous materials starting from mixture of elemental powders. Constituent powders are alloyed by continuous grinding and crushing between powders and balls, and balls to wall of container. MA has a capability to produce non-equilibrium phases as well as novel crystalline and quasi-crystalline phases. In addition, MA allows alloying of elements that are difficult to alloy by other methods (Suryanarayana, 2001)

The MA process was developed by John Benjamin in the 1960's at the International Nickel Company"s Paul D. Merica Research Laboratory. The original goal of the project was to produce a nickel-based superalloy for gas turbine applications. After multiple failed attempts, Benjamin proposed to use a high energy mill to plastic deformation and cold welding, and produce a refined internal structure. The eventual result of this endeavor was an oxide dispersion strengthened superalloy, attributed to MA (J. S. Benjamin, 1970). Benjamin"s work led to production of yttrium oxide and gamma prime hardening in a complex nickel-base superalloy, a small high speed shaker mill and eventually a larger ball mill to produce oxide dispersion strengthened alloys (ODS) on an industrial scale. MA became available to produce other ODS alloys, for coating applications and fast corrosion applications (Gilman & Benjamin, 1983).

MA's advantages were shortly described in the beginning. To replace the traditional method of long time annealing MA is proven very effective. Especially for the P type skutterudite cases where annealing is critical to form skutterudite phase. Generally to produce the skutterudite phase it takes 7-14 days annealing. And for some cases it takes even more. But BM can reduce the grain size and can produce fine powders which can able to form skutterudite phase after heat treatment. (Jie et al., 2013) stated that by using ball milling they were able to produce the high quality double filled skutterudite without the help of annealing. The total procedure was reduced from the traditional 7 days to 2 days. Moreover it helped to breakdown the ingot into nano-sized grains which helped the filler atom to travel less distance, they achieved the ZT 1 at 750K which is as same as the traditional method of sample preparation by annealing. But it is also evident that there should be a proper ball milling time to prevent aggregation. Longer BM for more than necessary tends to aggregate particles reducing the effect, and this is an aspect that can be systematically explored through investigation of the ball milling parameters.

2.5.1 Mechanism of alloying

The basis of MA is the cycle of powder particles that are repeatedly flattened, cold-welded, fractured and re-welded. When grinding balls collide, some amount of powders is trapped between them. This trapped powder undergoes two processes. The first is plastic deformation, which causes work hardening, failure and a reduction in particle size. The second is cold-welding that takes place due to the new surfaces created by the fractured particles, causing an increase in size. These two processes will eventually balance and the powder will come to an equilibrium particle size. As this process continues, particles become more homogenous, until eventually the final powder is a single phase. Steady state is reached when composition of every powder particle is the same as the proportion of the elements in the mixture of starting powders. Grain size decreases exponentially with time and can reach grain sizes on the nanometer scale. Because of this refinement ability, MA is extensively used for nanocrystalline material production (Koch, 1993) (P.-Y. Lee, Yang, & Lin, 1998). An additional effect that accompanies grain refinement is an induction of mechanical strain within the sample (Zakeri, Allahkarami, Kavei, Khanmohammadian, & Rahimipour, 2009). As particles are repeatedly flattened, lattice strain accumulates and plateaus. There are three different combinations of metals and alloys that are often used in MA: (i) ductile-ductile, (ii) ductile-brittle and (iii) brittle-brittle. Benjamin and Volin were the first to describe the mechanism of alloying on a ductile-ductile system (J. Benjamin & Volin, 1974). The ductile components become flattened to platelet/pancake shapes and some quantity of powders becomes attached to the surface of the balls. This coating helps protect the system from contamination and prevents some wear on the surfaces of the balls. The flattened particles become work-hardened (increasing hardness) and fracture as brittleness increases. Benjamin also described a ductile-brittle system during the initial states of milling (Gilman & Benjamin, 1983). The ductile powder particles become

flattened, but the brittle particles become fragmented and embedded in the ductile particles. As the ductile particles become work-hardened they also fracture. Lee and Koch demonstrated this reaction by MA of Ni (ductile) and $NiZr_2$ (brittle), where after 15 min of MA, the flattened Ni strips were embedded in a granular $NiZr_2$ matrix (P. Lee & Koch, 1988).

2.5.2 Planetary ball mill

Planetary ball mills can charge a few hundred grams of powders at a time. The vials are arranged on a rotating support disk. They rotate around their own axes and around the axis of the support disk. The vials and the supporting disk rotate in opposite direction which pins the grinding balls to the side of the vial. The balls rotate inwards, toward the center of the support disk, but eventually are overcome by the centrifugal force of the rotating support disk and travel across the diameter of the vial and impact on the opposite side of the vial. Planetary ball mills are able to produce higher velocities than a SPEX shaker mill, but frequency of impacts is much lower. Planetary ball mills are lower energy than a shaker mill. Planetary Ball mill used by (D. Chen, Ni, & Chen, 2007) was able to produce nano grain sized powders (30-80 nm) and the use of the iron balls in the vials played a key role for the Fe_3O_4 as stated in the paper. For the TE materials BM is new attraction for various advantages. The process is also very simple.

Reactant elemental or compound powders along with balls are needed to be charged into a milling vial maintaining a certain weight ratio between balls and powders. The vial is then loaded into a ball mill and rotated along the axis of the vial and at the same time the wheel is also rotated at a same 30 rpm speed. During ball milling the powders are subjected to a series of impact collisions between the powders and ball bearings as the ball mill constantly agitate the vial (Stordeur & Rowe, 1995) , (Suryanarayana, 2001). Resulting cold welding and fracturing of the powders leads to the formation of nanostructured domains.

2.5.3 Process variables

There are many variables that contribute to mechanical alloying. Manipulating some or all of the following variables will help lead to the desired phase or microstructure.

2.5.3.1 Type of mill

As discusses in the previous section, there are many types of mills that differ in sample size, ball speed, frequency of collisions and energy level. Minutes in a higher energy mill can produce the same result as hours in a lower energy mill. Yamada and Koch demonstrated this in comparing TiNi samples milled with a SPEX shaker mill and a vibratory mill (Yamada & Koch, 1993). The SPEX mill produced rapid grain size reduction when compared to the vibratory mill. Shaker mills can be used to screen for alloy production and then a lower energy/larger capacity mill, such as an attritor or commercial mill, can be used to produce larger quantities of a sample.

2.5.3.2 Ball milling container

Milling containers come in different shapes and are made of different materials. The choice of container is important, as it is a source of contamination. Softer containers can allow for material to become dislodged from the inner walls of the container and incorporated into the powder. Common milling container types are hardened steel, stainless steel, hardened chromium steel, tempered steel, WC-Co, WC-Co lined steel, and bearing steel. Shape of the vial also can affect milling efficiency. Harringa et al. using Si 80Ge20, showed that a SPEX shaker mill with a flat ended vial allowed alloying at a higher rate, in about 9 hours; while in a rounded end vial it took about 15 hours (Harringa, Cook, & Beaudry, 1992).

2.5.3.3 Ball milling speed

Milling speed is directly related to the energy input to the powder, but has some limitations. For rotating mills, there is a maximum speed, above which, balls become pinned to the sides of the milling container, and impacts are significantly reduced. Also higher speeds can produce higher temperatures, which can be undesirable (or be desirable, depending on the application). Calka el al. demonstrated this effect by milling vanadium and carbon (VC) at different energy levels, which produced different final products (Froes, 1990) Calka showed at medium energy, samples would form a nanostructure, but required a heating cycle to become an ordered VC compound. High energy resulted directly in a VC compound by milling.

2.5.3.4 Ball milling duration

The milling duration required to achieve a desired phase depends on how efficiently the mill can transfer energy to the sample. This is directly influenced by the type of mill used, the intensity of the milling, the ball-to-powder ratio, and the temperature of milling. Milling for too short of a time will not allow the reaction to finish, but milling for an excessive amount of time may result in an increased level of contamination or a completely different product.

2.5.3.5 Grinding medium and ball to powder weight ratio

Grinding balls are often made of steels and WC-Co due to their density and durability. Using a grinding container of the same material will also avoid cross contamination. During milling, powder can become coated to the balls and sides of the vial, which decreases the final yield. Using a combination of large and small balls can avoid excessive build up, as noted by Takacs and Pardavi-Horvath who were able to reduce the buildup of Zn on the walls of the vial by using smaller balls (Takacs & Pardavi-Horvath, 1994) Ball-to-powder ratio influences the amount of duration which takes to complete the

milling process. Higher energy mills can handle a lower ball-to-powder weight ratio due to the number of impacts that take place. An increase of ball-to-powder weight ratio causes the reaction to take place more quickly than a lower ratio (El-Eskandarany, Aoki, Itoh, & Suzuki, 1991). An increased weight proportion of the balls increases the number of collisions per unit time per volume of powder, which increases the rate of energy transfer from the milling device to the sample and consequently the rate of alloying.

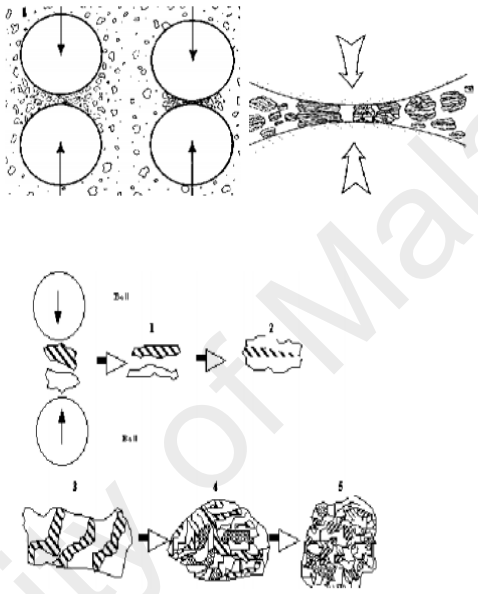

Figure 2.9: Mechanism of Alloying, Cold welding and fracture (Bux, Fleurial, & Kaner, 2010).

2.5.3.6 Process control agent

Process control agents (PCA), which are often organic compounds such as ethanol or hexane, can be added to the milling container to help control the rate of cold-welding and to prevent oxidation od the sample. This is desired in a system that has the propensity to cold-weld but not fracture. This effect can cause a buildup of welded particles and an imbalance to the system. Lee and Kwun used PCAs to control the buildup of welding by the ductile components in their Ti-Al system (W. Lee & Kwun, 1996). They reported that as the amount of PCA increased, the mechanism of MA changed from substitutional

diffusion to a penetration of metallic atoms into interstitial sites, the latter playing an important role in formation of an FCC phase.

2.5.3.7 Milling temperature

The temperature of milling can affect the rate at which a reaction takes place. The temperature can be lowered by dripping liquid nitrogen on the milling container or raised by heating the container. Milling at lower temperatures has the effect of further refinement of grains, and in some cases, increased likelihood of amorphous phase production (Ryu, Kim, Kim, & Moon, 2003).

2.5.3.8 Milling atmosphere

Milling atmosphere can influence the purity of the powders during a reaction. Depending on the materials, care must be taken to ensure that the starting powders do not react with the atmosphere. Nitrogen has been found to react with metal powders and for this reason is not often used in MA (Suryanarayana, 2001). Inert gases such as high purity argon are often used to ensure no unexpected reaction takes place. Vials can be filled and sealed in a closed atmosphere glove box, and then milled in a standard air atmosphere.

2.6 Spark plasma sintering

The Hot Press sintering process has some limitations which are higher costs, commonly due primarily to limited shape capabilities and long duration process resulting in a grain growth. Therefore, a spark plasma sintering (SPS) was developed as a potential powder consolidation method to obtain fully density materials at lower temperature in a short sintering duration, which can prevent the formation of deleterious intermediate phases and prevent grain growth. SPS was emerged during 1990s which was developed based on the idea of using the plasma on electric discharge machine for sintering ceramics in the early 1960 by Inoue (Kiyoshi, 1970).

The commercial SPS machine usually uses high alternating-current pulses passing through the powder compact along the pressure direction. The advantage of the current activated sintering technology is the capability to compact the powders into a dense bulk within several minutes owing to the self-heat effect (for materials like semiconductors and metals) and plasma effect (for material like insulators) generated by the current (W. Liu et al., 2012), as shown in figure 2.10. SPS systems offer many advantages over conventional systems like hot-press (HP) sintering, hot- isostatic pressing (HIP) or atmospheric furnaces, including ease of operation and accurate control of sintering energy as well as high sintering speed, high reproducibility, safety and reliability. The SPS process is expected to find increased use in the fabrication of functionally graded materials (FGMs), intermetallic compounds, fiber reinforced ceramics (FRC), metal matrix composite (MMC) and nanocrystalline materials, which are difficult to sinter by conventional sintering methods. Additionally SPS is not only used for the purpose of "sintering" but also of "bonding", "synthesizing" and "surface modification". For more details and examples of the utilization of the SPS method could refer to (Munir, Anselmi-Tamburini, & Ohyanagi, 2006).

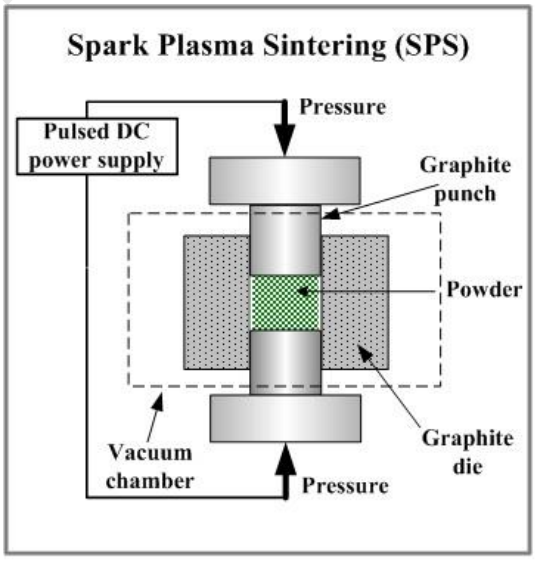

Figure 2.10: A schematic illustration of SPS technique for sintering TE materials (Kopeliovich).

The reduction in grain size following by densification process creates extensive interfacing between the compacted nanoparticles which can lower the thermal conductivity. The sintering samples can exhibit certain benefits over techniques that create very large-grain or single crystal materials, such as reduced thermal conductivity (due to enhancing phonons scattering at grain boundaries), increase power factor (due to electron filtering at grain boundaries), better mechanical prosperities and improve isotropy. In addition, bulk nanostructured samples are a relatively low-cost method to provide the large volume of materials which are necessary for more wide spread adoption of TE technology. However, a major challenge is obtaining complete removal of any binder or organics used in grinding, milling or wet chemistry processes, and obtaining as close to 100% of theoretical density after compaction. If this is not achieved, the carrier mobility will be substantially reduced by one or more orders of magnitude for just a few percent decrease in density, resulting in degraded the ZT (Vineis, Shakouri, Majumdar, & Kanatzidis, 2010).

CHAPTER 3: METHODOLOGY

3.1 Introduction

The aim of this chapter is to illustrate the experimental procedures has been used for the preparation of the samples, the material used, synthesis process and characterization process of those materials. The process is illustrated in a flow chart Figure 3.1. For the study at first powdered raw materials were mixed in a stoichiometric ratio and mechanically alloyed by ball milling. This is followed by compacting with cold press and heat treatment like vacuum furnace or compacting with SPS. X-ray diffraction (XRD), scanning electron microscopy (SEM), field emission scanning electron microscopy (FESEM) techniques were used to examine the structural and morphological characterizations for the compositions, respectively. TE properties were studied after successfully developing skutterudite phases and checked by XRD. ZEM -1 instrument was used to study electrical resistivity and Seebeck coefficient. Laser flash was used to calculate thermal conductivity. Successful skutterudite formulations was then studied by Jana 2006 software to determine the filling level of Bi in the $FeCo_3Sb_{12}$ skutterdite.

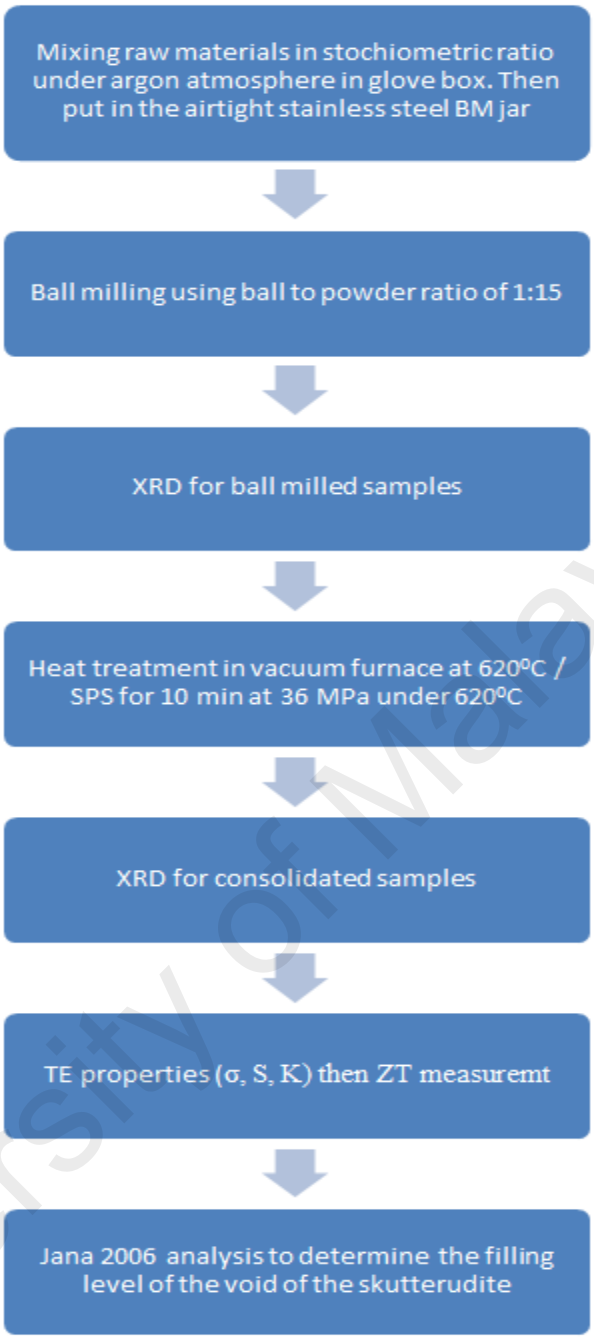

Figure 3.1: Flowchart of material preparation and characterizations.

3.2 Materials used for this study

In this experimental procedure, high purity raw materials as the form of powder being used to synthesize the binary, ternary and finally the quaternary skutterudites. The purity and the properties of the powders used for this study are described below.

3.2.1 Bismuth

Bismuth is a white, crystalline, brittle metal with a pinkish tinge. Bismuth is the most diamagnetic of all metals, and the thermal conductivity is lower than any metal. The purity of Bi was 99% which was used for this study. It was bought from Sigma Aldrich. Some of the major properties of Bi are listed below in Table 3.1

Table 3.1: Bismuth's properties.

Element	Properties
Bismuth (Bi)	Atomic Number 83 Atomic Weight 208.98 Melting Point 271.5^0C Boiling Point 1564^0C Density 9.8 g/cm^3 Electronegativity 2.02

3.2.2 Iron

Iron is a relatively abundant element in the universe. The pure metal is not often encountered in commerce, but is usually alloyed with carbon or other metals. The pure metal is very reactive chemically, and rapidly corrodes, especially in moist air or at elevated temperatures. 99.9% purity of Fe powder was used for this experiment and was ordered from MERCK. Some of the major Fe properties are listed in the table 3.2 below.

Table 3.2: Iron's properties

Element	Properties
Iron (Fe)	Atomic Number 26 Atomic Weight 55.845 Melting Point 1538^0C Boiling Point 2862^0C Density 7.874 g/cm^3 Electronegativity 1.83

3.2.3 Cobalt

Cobalt is a brittle, hard, silver-grey transition metal with magnetic properties similar to those of iron (ferromagnetic). From Alfa Aesar 99.998% pure cobalt powder was bought to use in this experimental procedure. Few key properties of Co are listed in the Table 3.3:

Table 3.3: Cobalt's properties

Element	Properties
Cobalt (Co)	Atomic Number 26 Atomic Weight 55.845 Melting Point 1538^0C Boiling Point 2862^0C Density 7.874 g/cm^3 Electronegativity 1.83

3.2.4 Antimony

Metallic antimony is an extremely brittle metal of a flaky, crystalline texture. It is bluish white and has a metallic luster. It is not acted on by air at room temperature, but burns brilliantly when heated with the formation of white fumes. It is a poor conductor of heat and electricity. The Sb used in this study has the purity of 99.5% which was bought from Alfa Aesar. Some of the Sb properties are listed below in the Table no 3.4.

Table 3.4: Antimony's properties

Element	Properties
Antimony (Sb)	Atomic Number 51 Atomic Weight 121.76 Melting Point 630.63^0C Boiling Point 1635^0C Density 6.697 g/cm^3 Electronegativity 2.05

3.2.5 Lanthanum

Lanthanum is a very reactive rare earth material. It oxides with the air rapidly and need to be handled delicately under vacuum environment due to its rapid reactive behavior. La's major properties are listed in the Table 3.5.

Table 3.5: Lanthanum's properties

Element	Properties
Lanthanum (La)	Atomic Number 57 Atomic Weight 138.91 Melting Point 920^0C Boiling Point 3464^0C Density 6.162 g/cm^3 Electronegativity 1.10

3.2.6 Copper

Copper is a unique and one of the few material which appear in nature as directly usable form. Copper has bright metallic luster with reddish appearance. It has very high electrical and thermal conduction properties. It is not particularly reactive material. Some of the key properties are listed below in the Table 3.6.

Table 3.6: Copper's properties

Element	Properties
Copper (Cu)	Atomic Number 29 Atomic Weight 63.546 Melting Point 1084.62^0C Boiling Point 2562^0C Density 8.96 g/cm^3 Electronegativity 1.9

3.3 Ball milling

Ball milling process is used for the mechanical alloying of the elements used for the experiments. This method will be useful to attain micron sized particles needed for this research, where the thermoelectric properties will be improved by micrstructuring. Retsch

PM-100 BM machine was used for the milling process. Ball milling is used to prepare samples by using high energy ball milling technique. Inside the jar sequence of high energy collisions helps to occur mechanical alloying. Ball milling technique is easier and less time consuming compare to other methods as described in the table 1.1. It is also an effective method to prepare contamination free powder samples under high purity argon gas atmosphere. The stoichiometric materials were loaded into a stainless steel jar with stainless steel balls. 300 rpm speed with 15 min run time and 10 min stop time with reverse rotation was maintained throughout the milling process to prevent heat generation during high speed milling. The loading and unloading of the materials was done inside the glove box under argon atmosphere to avoid contamination and the stainless steel ball milling jar is air tight to prevent contamination during milling process.

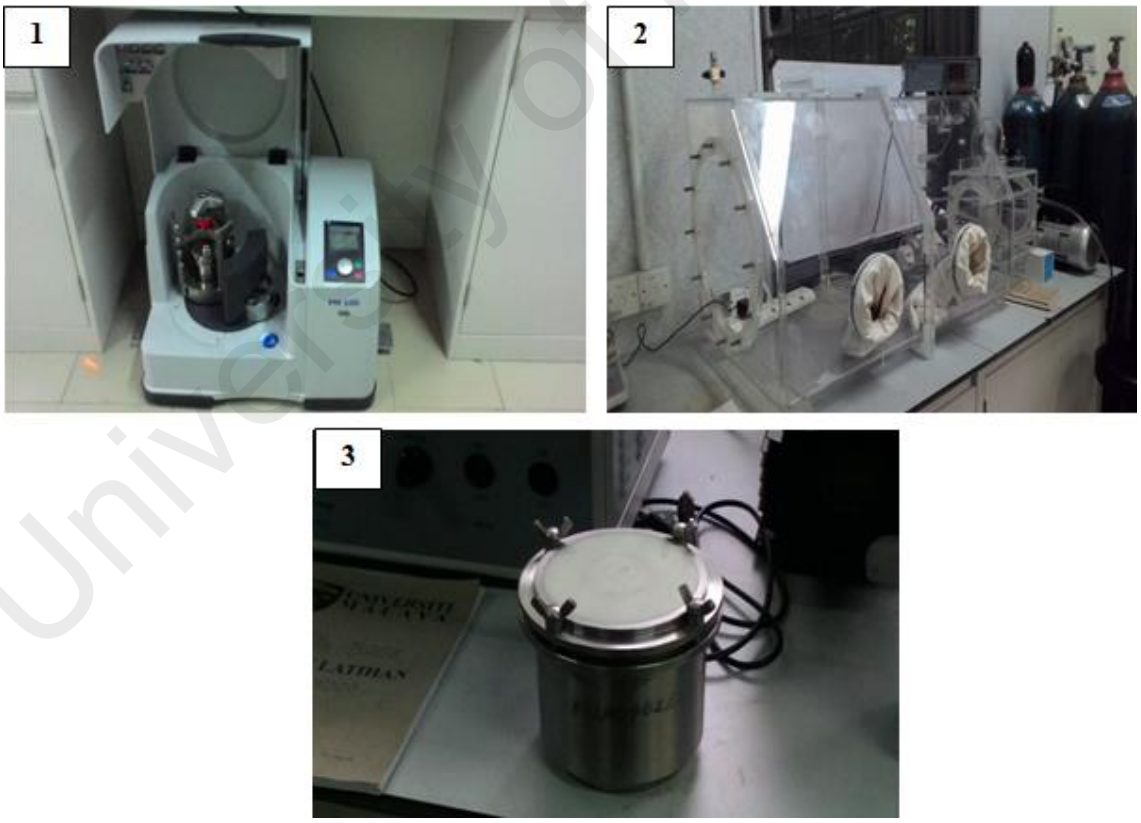

Figure 3.2: 1) Retsch PM-100 BM machine, 2) Glove Box, 3) Ball Milling Jar.

3.4 Consolidation process

3.4.1 Cold pressing

To make solid samples for sintering, as milled powders needs to be compacted and solidified into a particular shape. This will provide a high pressure method to consolidate the material into the desired crystal configuration. For this purpose a cold press was used. The milled powders were compacted under room temperature using hardened SS steel die at 375 MPa pressure for 5 min. The pellet size is 10 mm in diameter and thickness of 2 mm (approx.)

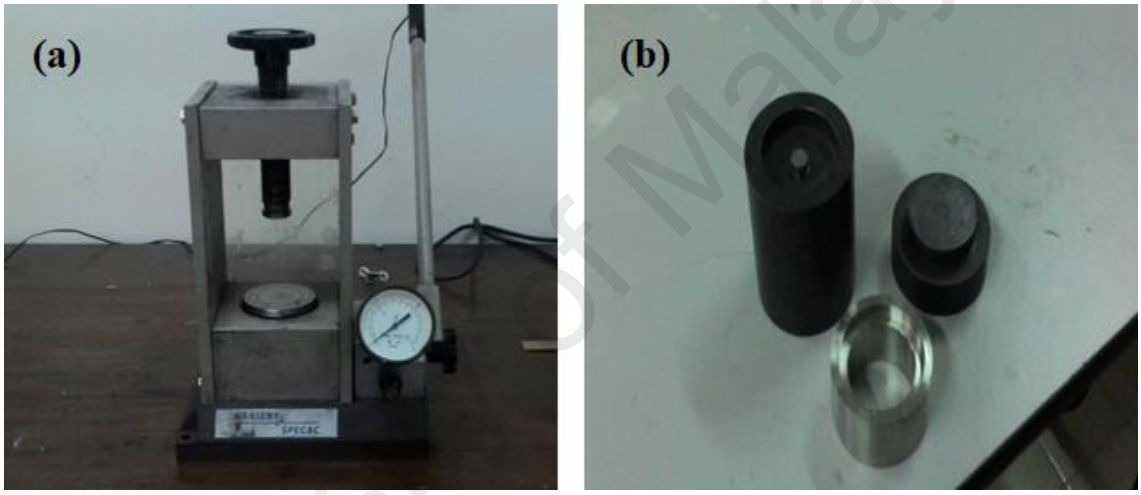

Figure 3.3: (a) Manual Cold press and (b) Hardened SS steel die.

3.4.2 Sintering using tube furnace

MILA-5000 from ULVAC was used to sinter the samples. In this case, the high heat during the sintering is expected to consolidate the powder into the desired crystal structure. It has infrared heating technique with precision temperature regulation. The compacted samples were placed on a quartz tube holder and put inside the quartz tube furnace. Then the samples were sintered under 5 Pa vacuum in 620^0 C for 2 h. The heating rate was used as 4^0 C per minute increment from room temperature to the set point.

3.4.3 Spark Plasma Sintering

Spark Plasma sintering (SPS) was used to make more dense samples for this study. SPS is a state of the art sintering technique. In the spark plasma sintering high pressure and heat was applied to the BM powder samples at the same time. Ultimately,this is the most desired process to consolidate the powder into a bulk crystal structure using high pressure and high temperature. This process was able to form dense samples with less grain growth. 36MPa pressure was used and the samples were sintered at 620^0C for 10 min. The heating rate was fixed at 100^0 C/min. Sample size was standard 10 mm diameter with 2 mm thickness. The sintering process was done under argon atmosphere. A sintering atmosphere of ~4 Pa vacuum was used in order to evacuate ambient air from the mold. After SPS the samples were mechanically cut using a cutting machine into bar shaped sizes for TE measurements. The fabricated samples shows high density compared to vacuum sintered samples. Density measurement was conducted using Archimedes method.

3.5 Characterizations

3.5.1 X-Ray Diffraction

X-Ray diffraction technique was used to determine the phase formation after ball milling and sintering. It is widely used in phase identification of a crystalline material. Besides, the lattice parameter information can also be determined by Jana 2006 software. The x-ray generator used a copper source to produce X-rays with a characteristic wavelength of 1.54060º A. The voltage and current we used for X-ray generation are 45 kV and 40 mA, respectively. An XRD scan 2Θ degree was performed in between 5 to 120 degree. Reitveld refinement and phase determination was performed with commercial software (HighScorePlus version 3.0c, PANalytical B.V., Almelo, The Netherlands).

3.5.2 SEM analysis

The morphologies of powders and the fracture of bulk samples were observed by scanning electron microscopy. Powder samples were spread on the conductive tape which was placed on a sample holder head. Loose powder on the tape was removed by air blower. After that the head was inserted into sample holder maintaining approximately 2mm gap between sample surface and the upper surface of the sample holder. Afterwards the sample holder was placed in machine for imaging and EDS and turn on the electron mode. Then adjusting focus, brightness and contrast, images were taken at various magnifications. Imaging was done on 20kV and Image mode.

After taking SEM image, elemental analysis was done. Then, again adjustment of focus, brightness and contrast were done. Several points in the selected area were nominated for quantitative elemental analysis. Some element mapping area also selected for quantitative elemental analysis. The system automatically runs the quantitative analysis at every selected points and mapping area according to the selection sequence.

3.5.3 Thermoelectric properties analysis

To analyze the thermoelectric properties, Seebeck coefficient, thermal conductivity and electrical conductivity was measured. ZEM 1 was used to measure the Seebeck and the electrical conductivity. Laser flash was used for the thermal conductivity analysis.

Electrical conductivity is not measured directly by the ZEM 1, actually the measurement of the electrical resistivity of the thermolelectric materials as a function of temperature was performed using the ZEM 1 instrument. Electrical resistivity is reciprocal of electrical conductivity.

The Seebeck coefficient is known as the thermopower (S) of a material. It states that the amount of potential induced by thermoelectric voltage regarding to the temperature gradient across the sample. Seebeck measurement also carried by the ZEM 1 instrument.

Thermal conductivity was measured by using laser flash method. The laser flash method can determine the thermal conductivity of a sample from its thermal diffusivity, density and specific heat. The density of the samples was measured by the Archimedes method.

CHAPTER 4: RESULTS AND DISCUSSION

The goal of this chapter is to present the characterization results of the skutterudite materials and prior to achieve the final results what are the procedures and process parameters were used to achieve the final goal. Followed by the Jana 2006 software results to show the occupancy of the void of the resultant skutterudites. In this study SPSed samples of $Bi_{0.6}FeCo_3Sb_{12}$ has the TE characterization due to the successful fabrication of skutterudite phases. The characterization samples would be discussed individually in terms of their microstructural and thermoelectric properties along with the other formulations, process parameter, ball milling time optimizations and Jana 2006 software results.

4.1 Ball milling optimization to prepare binary skutterudite

Milling time optimization is a trial and error based experiment. To get the optimum results a series of trial and error based ball milling process was conducted to achieve skutterudite phase and homogenous particle distribution. Because each material has different properties and depend on those properties the BM time changes. Figure 4.1 shows the XRD pattern of comparison among the BM hours for the formation of binary $FeSb_3$ skutterudite. Longer ball milling hours was studied to achieve $FeSb_3$ skutterudite phase through mechanical alloying. It is evident that the longer BM hours was not suitable for the binary skutterudite formation using BM. Longer BM was unable to form the desired $FeSb_3$ phases. Instead only the Sb peak and of secondary $FeSb_2$ phase were present as the impurity phase. $FeSb_3$ skutterudite phase formation was not present even after running 55h BM. A series of trials to figure out the optimum BM time for unfilled skutterudite was studied and the results was not successful.

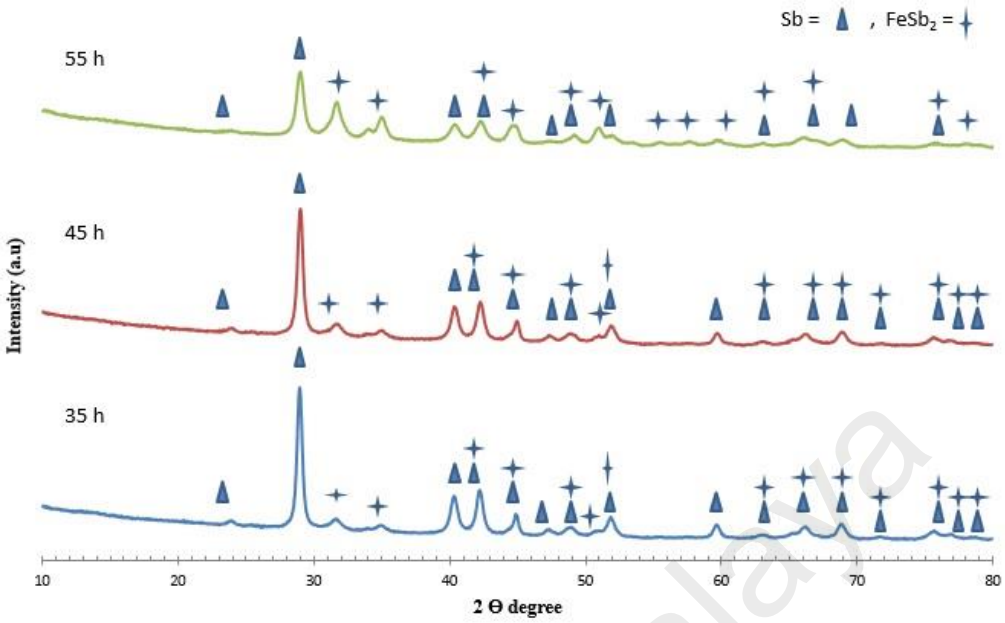

Figure 4.1: Comparison among the BM hours to study different BM duration to form binary $FeSb_3$ skutterudite

4.2 Process control agent subtraction

After many unsuccessful attempts of synthesize the binary skutterudite through BM, process control agent (PCA) was introduced for the formation of the skutterudite phase. PCA have been added to powders in order to retain the equilibrium state between welding and fracturing processes. Due to the fact well known that during ball milling process of processing powders- the repetitive cold welding, fracturing and re-welding process has high possibility to get imbalanced. The scope of process control agent was studied to see the effect on the skutterudite phase formation with the BM time. Ethanol 0.1 wt% was used as process control agent. At first it was studied only with the $FeSb_3$ as shown in figure 4.2. But there was no evidence of the phase formation for the binary $FeSb_3$ skutterudite. Which later influenced to introduce fillers in the skutterudite structure.

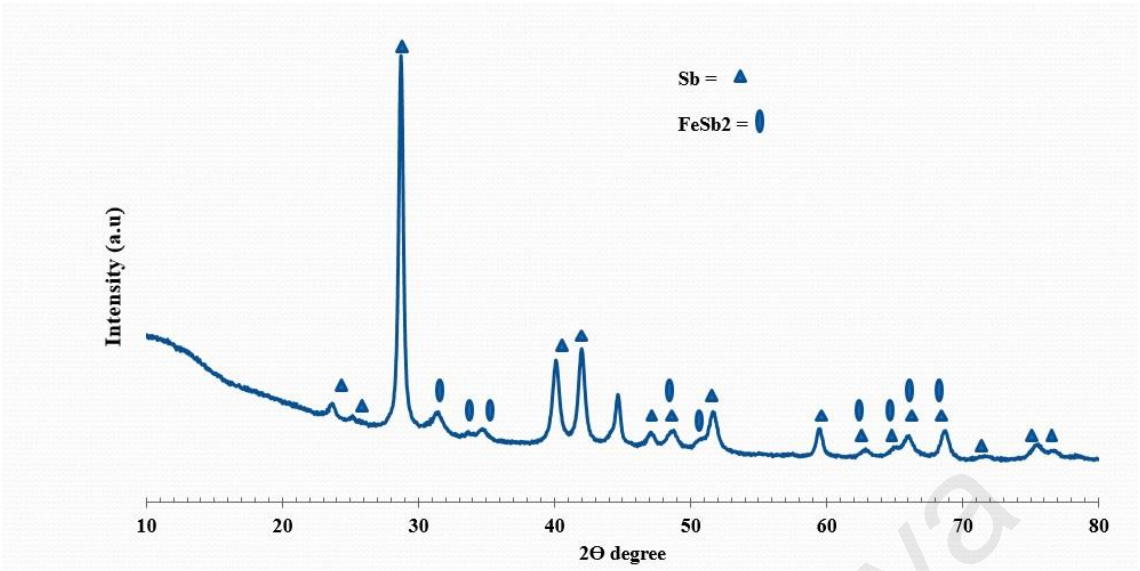

Figure 4.2: 35h BM Fe_4Sb_{12} powder with 0.1 wt% ethanol as process control agent.

Bismuth as filler was introduced. The Moller ratio of ethanol was kept same as process control agent. In Figure 4.3 we can observe the XRD pattern which indicates even after the introduction of the filler in the formulation no significant changes occurred. Only reduction of $FeSb_2$ peaks was observed.

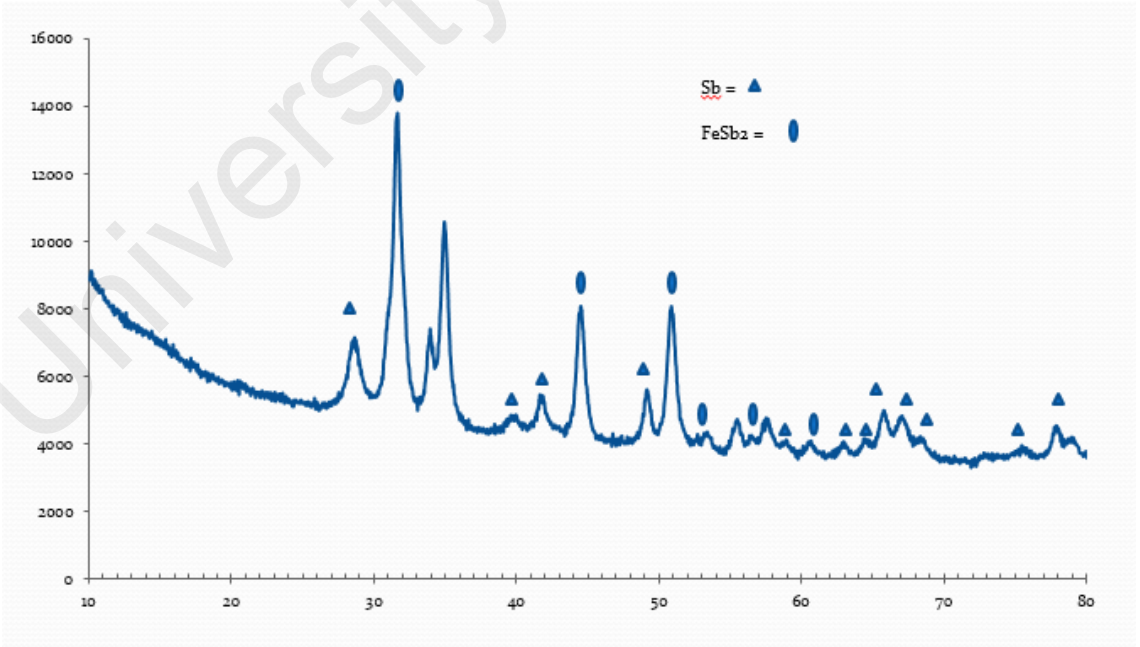

Figure 4.3: 35 h BM $Bi_{0.6}Fe_4Sb_{12}$ powder XRD with 0.1 wt% ethanol.

The results were unsatisfactory compared to the sample without the process control agent. XRD pattern in the figure 4.4 shows the peak shift to the right in comparison with the powder sample prepared by BM without ethanol (orange color). Antimony peak is reduced and the increase of $FeSb_2$ peaks is visible. This right shift actually indicates that the bismuth are being mechanically alloyed which might help to create skutterudite phase formation after heat treatment.

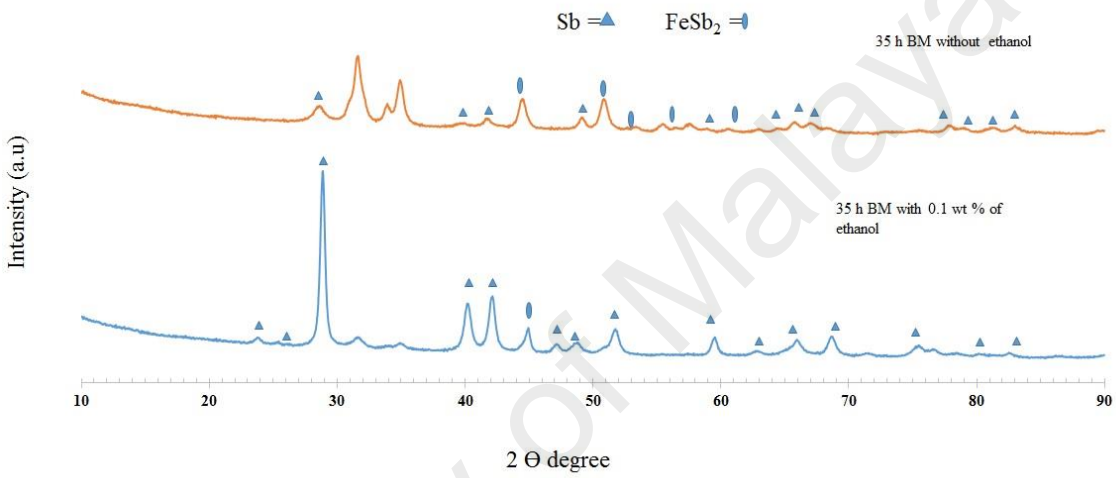

Figure 4.4: Comparison between $Bi_{0.6}Fe_4Sb_{12}$ formulation with and without ethanol as a process control agent.

The process control agent actually slows down the mechanical alloying inside the BM jar, which actually an obstacle in the formation of the skutterudite phase. Therefore discarding of the process control agent during the BM process is suggested.

4.3 Effect of the reduced ball milling time with filler and dopant

After a series of trials, different fillers were also studied along with Bi. Lanthanum (La) was used as filler in the as a formulation of La. In this study, the ball to powder ratio was also studied and 15:1 ball to powder ratio was chosen as the ideal one due to the fact that it helped to increase the skutterudite phase. In figure 4.5 shows the comparison among BM time with La as filler and also the effect between 10:1 and 15:1 ball to powder ratio. We were able to produce some skutterudite peaks by BM after removing process

control agent and introducing fillers in the skutterudite formulation. As shown in the figure 4.5 it has shown more skutterudite peaks for 35 h BM time and with the 15:1 ball to powder ratio.

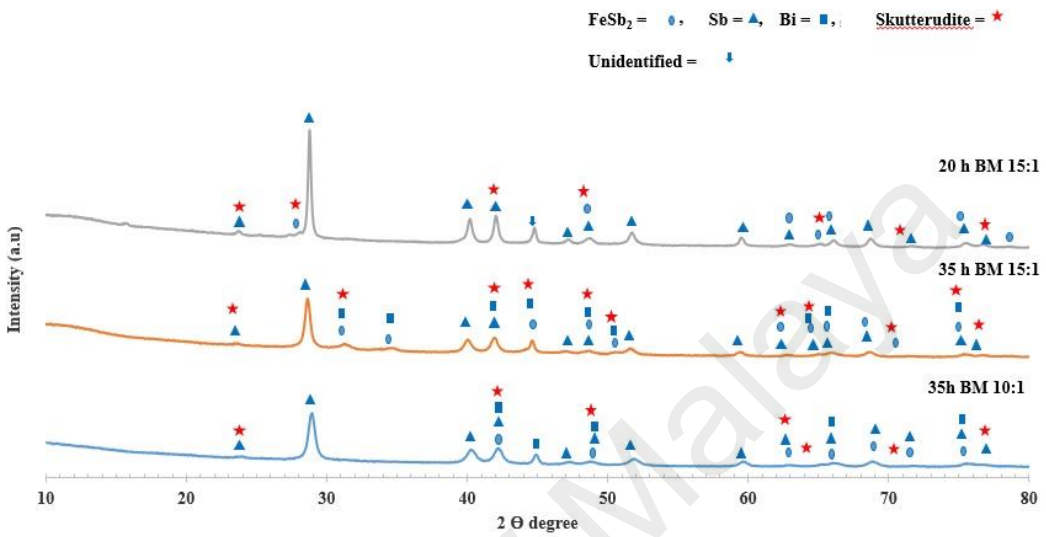

Figure 4.5: Comparison among BM $La_{1.5}Fe_4Sb_{12}$ samples with different preparations of ball to powder ratio and BM hours.

Effect of copper (Cu) and Bismuth (Bi) as a filler in the formation of skutterudite phase was also studied after the introduction of La. Cobalt (Co) was also introduced to substitute Fe in the skutterudite cage. Whilst the introduction of Copper (Cu) and Bismuth (Bi) as fillers with the Co substitution on Fe site has shown different results which helped to further reducing the BM timing and Co substitution level. XRD pattern in figure 4.6 is showing Cu as filler with Co substitution on the Fe site with 10 h BM time.

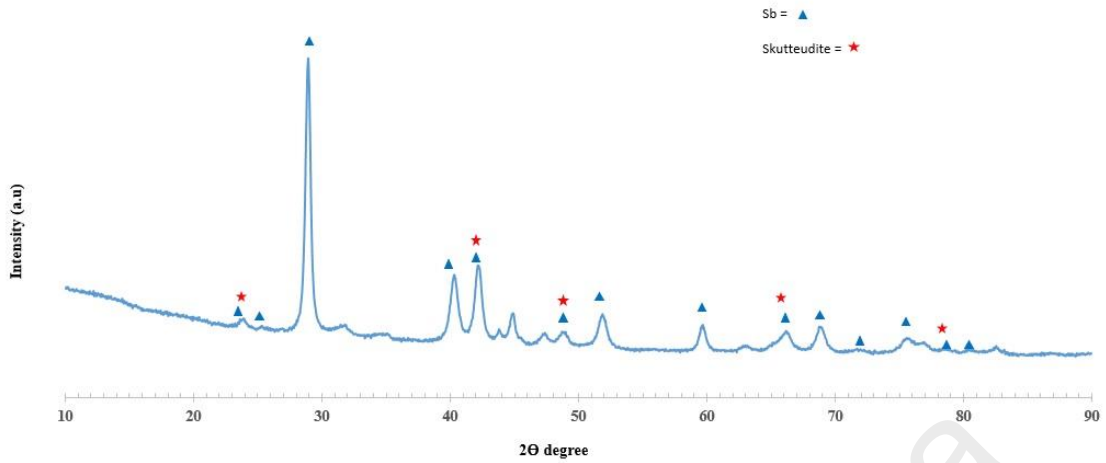

Figure 4.6: 10 h BM $Cu_{0.6}Fe_3CoSb_{12}$ powder sample's XRD.

Although the XRD pattern shows the successful formation of some skutterudite phase, still the Sb peak is much higher for the 10 h BM time. No phase shift was observed which indicates Cu as filler might not be the potential one as filler as its mass is small to take place in the skutterudite cage structure. Which is supposed to eventually lead to deform the lattice parameter. Furthermore, no phase shift in the XRD spectra is a clear indication that Cu is not acting as a filler atom. Also the skutterudite phase formation was significantly less in this duration of BM. Besides the substitution level of Co also appears to be not enough. As a result the BM duration was increased with substation level of Co on the Fe site was increased. XRD results of the comparison between the Co substitution, BM time increased and heavier filler is shown in the figure 4.7. The Sb peak intensity is decreased and the formation of the skutterudite phase was increased and after $La_{1.5}Fe_4Sb_{12}$ formulation for 35h BM time the $Bi_{0.6}FeCo_3Sb_{12}$ formulation exhibits potential skutterudite phase formation with less BM time.

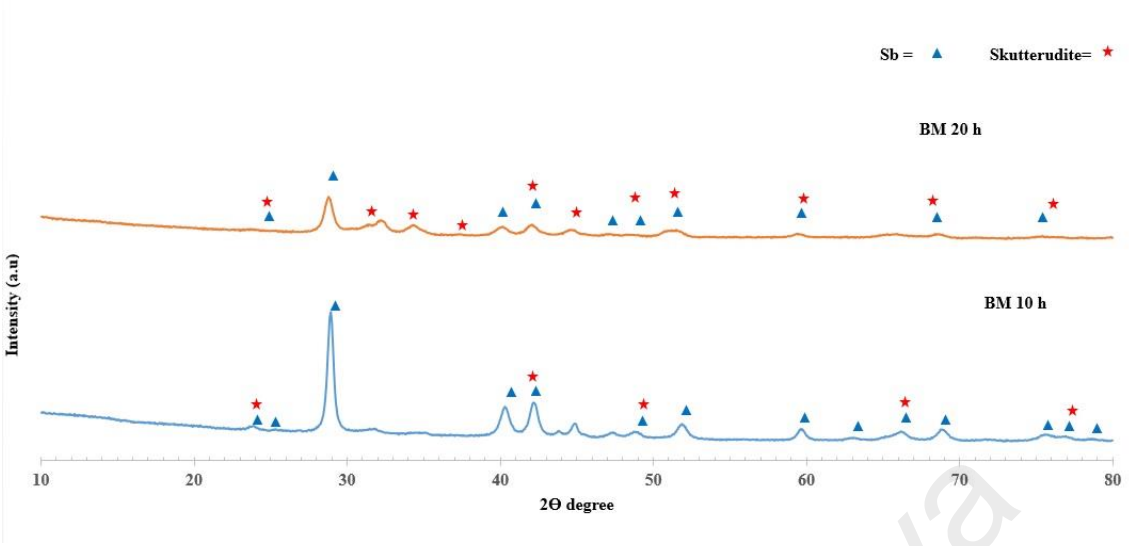

Figure 4.7: Comparison between the BM time and Co substitution. 20 h BMed XRD pattern has more skutterudite phase than the 10 h BM powders. For 20 h the formulation was used $Bi_{0.6}FeCo_3Sb_{12}$ where in 10 h $Co_{0.6}Fe_3Co_1Sb_{12}$ was used.

From figure 4.7 it was observed that the increase of Co helps to form more skutterudite phase. Skutterudite formulation of $Bi_{0.6}FeCo_3Sb_{12}$ for 20 h and 25 h BM time with Bi as a filler was studied to see the BM time optimization. The filling fraction level of Bi was kept 0.6. From the figure 4.8 the XRD pattern reveals 20 h BM time producing more skutterudite phases than the 25 h BM time. Therefore 20 h BM time was chosen for the sintering using MILA-5000 furnace.

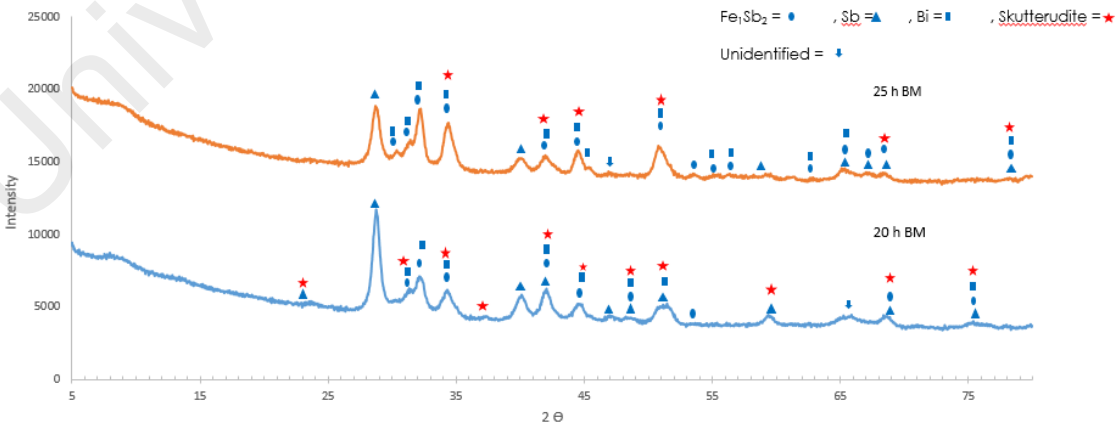

Figure 4.8: Comparison between the 20 and 25 h BM time of $Bi_{0.6}FeCo_3Sb_{12}$ skutterudite.

4.4 Sintering effect on the filled skutterudite system

Observing all the BM times' 20 h powder sample of the formulation $Bi_{0.6}Fe_1Co_3Sb_{12}$ was chosen for sintering. Slow heating rate (4^0C per minute) was introduced to give the sample more time for the reaction. MILA-5000 furnace was used for sintering. Figure 4.9 showing the comparison with the BM results of 20 h and 25 h samples with sintered sample. Using the binary phase diagram 620^0C temperature was selected for sintering.

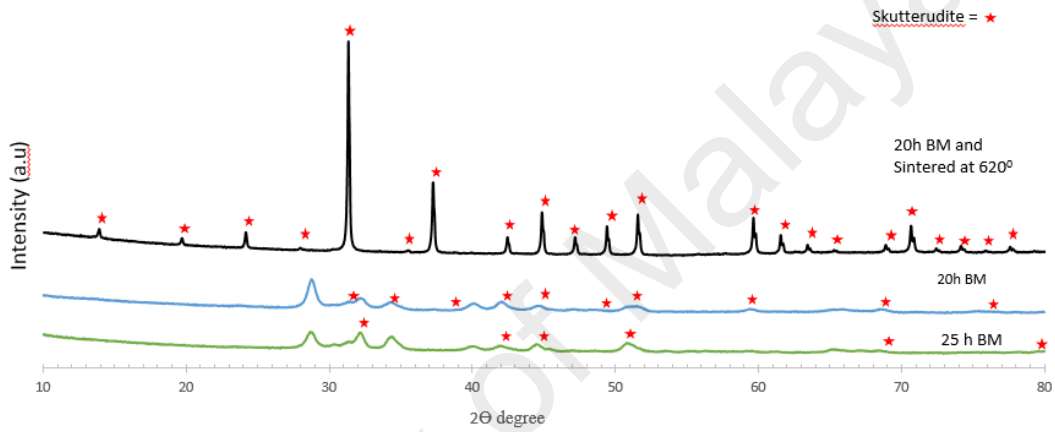

Figure 4.9: Comparison among 25 h (green line at the bottom) and 20 h (blue line in the middle) BM samples with sintered sample after 20 h (black line at the top) BM.

After the sintering for 2h at 620^0C the desired single phase skutterudite was obtained. From the XRD pattern in figure 4.9 it is evident that 20 h BM sample contained more skutterudite phase than the 25h sample. Thus it was chosen for sintering. It was sintered under vacuum atmosphere to prevent oxidization and impurities. Although there was a report of formation of the binary skutterudite phase by mechanical alloying (Junyou Yang et al., 2004). However, without the heat treatment of the sample it is very difficult to form the quaternary skutterudite phase let alone the single phase. After studying all the milling times presented, it was evident that shorter ball milling time is ideal to produce single phase skutterudite. Along with the substitution and filler in the skutterudite. Furthermore, the ball milling time optimization was studied. For this study 10 h, 15 h and 20 h ball

milling duration was chosen. The vacuum sintered samples showed less density (less than 90 %) which were determined by Archimedes method. Less dense samples are not ideal for TE property measurement so spark plasma sintering (SPS) was chosen to produce the denser samples due to the fact it is widely used for making dense samples.

4.5 Spark plasma sintering for denser skutterudite and Jana 2006 analysis with reitveld refinement

It is shown that the preparation of single phase skutterudite SPS was useful to produce dense samples for good thermoelectric properties. SPS process helps less grain growth during the heat treatment due to its fast heating rate. The result after SPS was more dense samples. The samples are more than 93% dense (highest density was 97% for 15 h BMed sample) with SPS compared with the vacuum sintered ones with around 85% density. Furthermore, single phase skutterudite samples were successfully prepared. The XRD spectra of the bulk $Bi_{0.6}FeCo_3Sb_{12}$ skutterudite for different milling time is shown in Figure. 4.10. A bulk skutterudite was formed for 10 h 15 h and 20 h spark plasma sintered samples. It has been found that the predominant phase of the skutterudite $CoSb_3$ (space group Im-3) were present for all the samples. A small peak of Bi is present in both of the 10 h and 15 h ball milled samples.

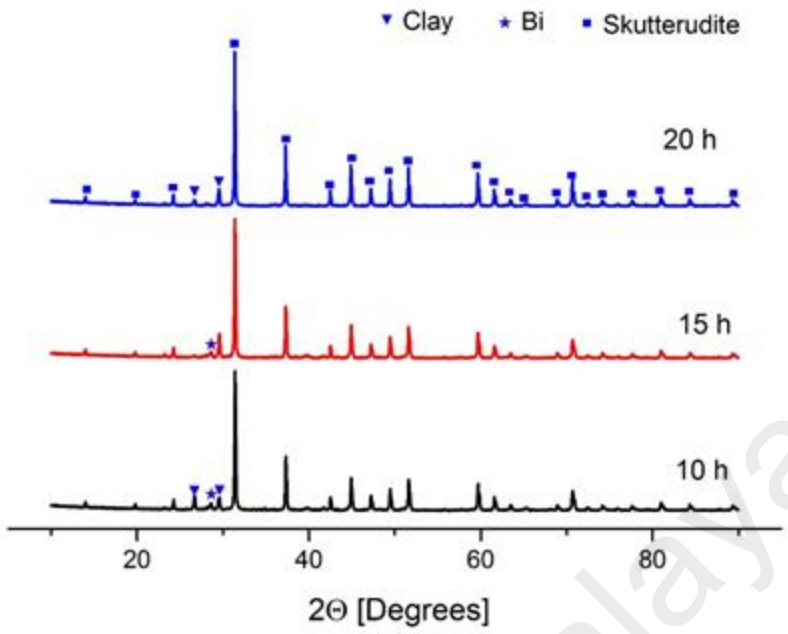

Figure 4.10: X-Ray diffraction pattern of the as SPS $Bi_{0.6}FeCo_3Sb_{12}$ for 10 h, 15 and 20 h ball milling duration.

Rietveld refinement analysis was carried out using Jana 2006 software to identify the crystal structure at room temperature. This method used for structural analysis of nearly all classes of XRD technique. The software refines various parameters including peaks' width and shape, lattice parameters, preferred orientation to derive a calculative diffraction pattern. The lattice parameter generated from the software is listed in Table 4.1.

Table 4.1: Lattice parameter of the $Bi_{0.6}FeCo_3Sb_{12}$ skutterudite for different milling duration. Their actual compositions after sps and Fe occupancy.

Ball Milling Duration	Nominal composition	Compositions calculated by Jana 2006	Fe Occ.	Lattice parameter (Å)
10 h	$Bi_{0.6}FeCo_3Sb_{12}$	$Bi_{0.28}Fe_{0.96}Co_{3.02}Sb_{12.02}$	28.2%	9.0499 (2)
15 h	$Bi_{0.6}FeCo_3Sb_{12}$	$Bi_{0.46}Fe_{0.99}Co_{2.99}Sb_{12}$	27.1%	9.0489 (2)
20 h	$Bi_{0.6}FeCo_3Sb_{12}$	$Bi_{0.44}Fe_{0.94}Co_{3.14}Sb_{12}$	27.1%	9.0499 (1)

The crystal lattice of $Bi_{0.6}FeCo_3Sb_{12}$ has been expanded for all the three ball milled samples compared with the unfilled Co_4Sb_{12} samples with the lattice parameter of 9.035 Å. This indicates that the Bi addition has filled the void of the Co_4Sb_{12}. In Figure 4.11 it

has been showed the crystal structure, distribution of the atoms in the lattice and their occupancy retrieved by Jana 2006.

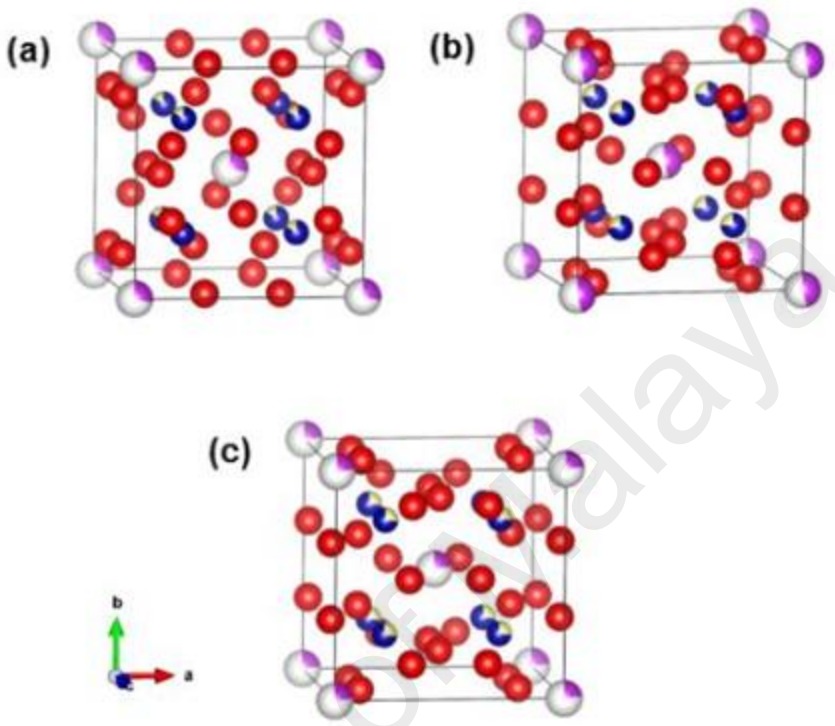

Figure 4.11: Crystal structure of the 10 h, 15 h and 20 h MA-SPS samples retrieved from Jana 2006.

It can be seen that the Bi dopant was successful in partially filling the voids of the skutterudite, which served as a thermal 'rattler' and hence reduced the overall thermal conductivity of the bulk skutterudite.

On the other hand, Fe dopant was able to partially substitute the Co sites in the skutterudite lattice, and hence the electrical conductivity was increased. This is attributed to the increased delocalization of the valence electrons of Fe compared to Co, due to the large atomic radius of Fe compared to Co, which are 156 pm and 1.25 Å , respectively. And also due to the valence state (Co and Fe: +2, and+3) and electron affinity (Fe = 15.7 kJ/mol and Co = 63.7 kJ/mol). These result agreed by a report carried out by Said et al (Said et al., 2017).

It can be also deduced from the Rietveld Analysis of all three formulations for different milling times, the actual composition of the skutterudite indicates that the Fe substitution is approximately constant, indicating that regardless of the milling time, a consistent substitution of Fe has occurred. On the other hand, for the 10 h milling time, the actual composition indicates that there is a lower filling ratio of Bi compared to the 15 h and 20 h milling times. This can be explained by the larger particle size of the 10 h milled samples, when then tend to be rejected by the skutterudite lattice during the SPS process. This is also supported by the observation of the formation of Bi secondary phase which are more prevalent in the 10 h sample. Details of the microstructure will be elaborated in the following section.

4.6 Field Emission Scanning Electron Microscopy (FESEM) and Scanning Electron Microscopy (SEM) with particle size analysis

The microstructure images of the powder samples were captured by FESEM and SPSed samples were captured by SEM. At first $Bi_{0.6}FeCo_3Sb_{12}$ sample's 10 h, 15 h and 20 h milling time samples were BM and then the powder pattern was studied with XRD and microstructure was observed with FESEM. Samples sintered with SPS was also studied with SEM and EDS for microstructure analysis and chemical mapping. Figure 4.12 showing the powder images which indicates the particle sizes after 10 h, 15 h and 20 h after ball milling. In the figure 4.12 10 h (a) and 20 h (c) samples shows they have different particle sizes which is observable with plain eyes. From very tiny particle size to bigger particle size distribution is observed for these two samples. Among the three samples 4.12 15 h (b) BM samples has the most even particle size distribution comparing to the 10 h and 20 h as milled powder samples. Which leads to the hypothesis, that although 20 h samples was chosen at the first for the vacuum sintering from the XRD pattern. But 15 h sample might be the potential one to optimize the factor of BM time. After these ball milling SPS was conducted for these powder samples. Followed by XRD,

SEM and TE property analysis. For the 10 h sample the in the figure 4.17 (a), SEM image showing conglomerated particles which was later found as Fe in the figure 4.17 (d) when chemical mapping was done. In the images (a) and (d) of figure 4.17 the conglomerated Fe is visible. 15 h BM and SPSed sample is showing a balanced distribution in the mapping which is shown in the figure 4.18. Bi (b), Co (c), Fe (d) and Sb (e) distribution in the figure 4.18 shows well distributed chemicals all over the sample. But the figure 4.19 image and mapping showing uneven distribution of chemicals and large pores are visible on the 20 h SPS sample. Comparing these microstructured images 15 h sample is the potential among these three SPSed samples for BM time optimization. The particle sizes of the SPSed samples were studied by particle size analyzer (Analysette 22 Nano Tec Plus by FRITSCH). Figure 4.12 which depict (a) ball milled particles at 10 h, (b) ball milled particles at 15 h, (c), and ball milled particles at 20 h, which are respectively magnified images at 20000 x magnification. Comparing the FESEM images it is observable that 15 h ball milling time has a more homogenous distribution compared to the 10 h and 20 h samples. By visual inspection, the particles for 10 h appear to be the largest, with the particles for 15 h being the smallest. In comparison, the particles for 20 h comprise of small particles (comparable in dimension to 15 h), but at the same time also demonstrate agglomeration into much larger particles in some clusters. More investigation was conducted on the particle sizes of these three BMed samples. Lower magnification for the microstructure was also observed to narrow down the possibility of the best particle size distribution followed by particle size analyzer. Figure 4.13 shows the 10000 x magnification of the 10 h, 15 h and 20 h BMed samples and through this we confirm that the 20 h sample shows a higher degree of agglomeration compared to the 10 h and 15 h sample.

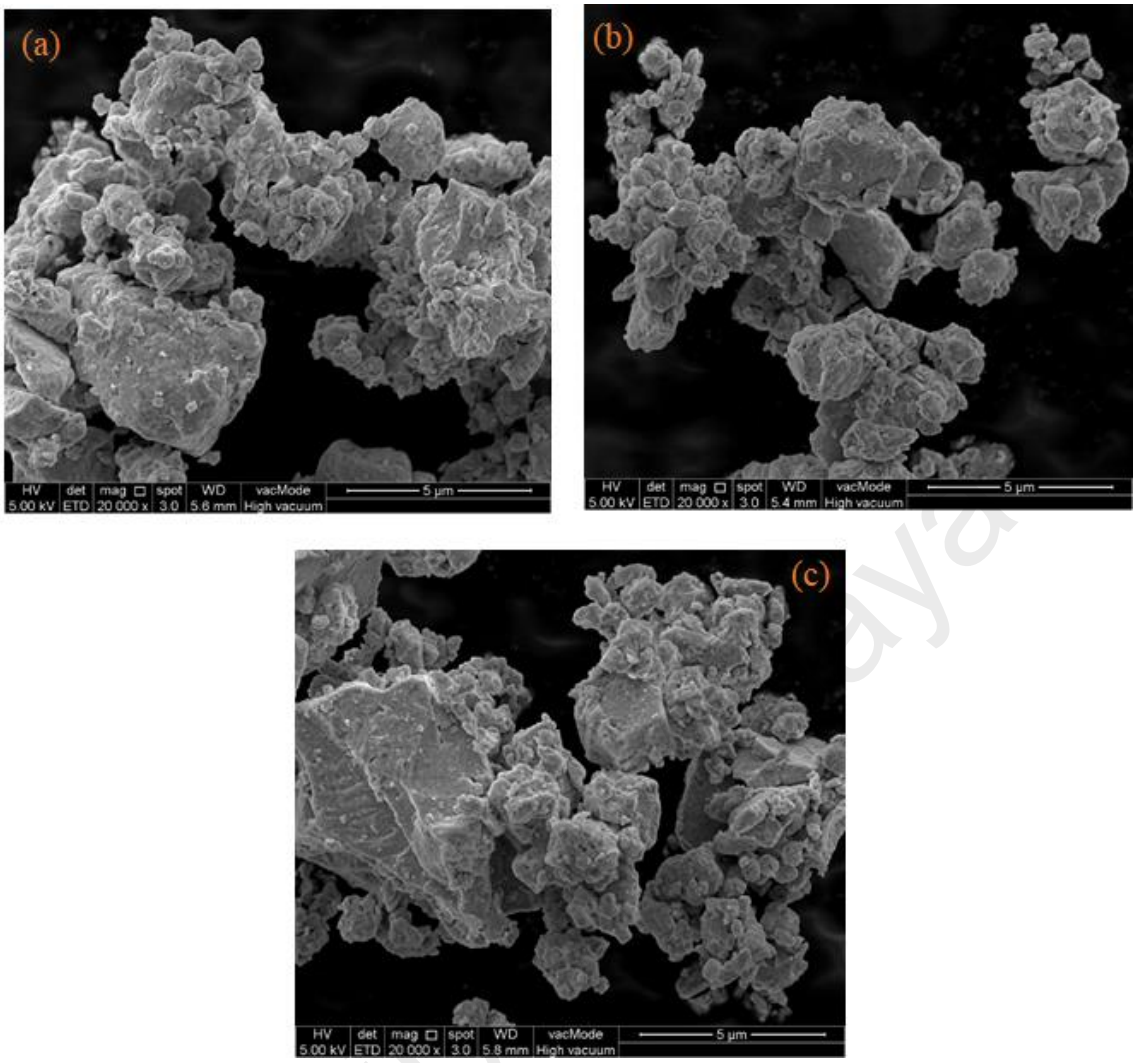

Figure 4.12: 10 h (a), 15 h (b) and 20 h (c) as-milled powder samples' FESEM images with 20000 x magnification.

Hence, we expect subsequent standard deviation of particle size of 20 h to be the largest amongst the sample, which should be reflected in the particle size analysis in Table 4.2. Besides FESEM images indicated that the 15 h mechanically alloyed sample provided the best grain size reduction, as supported by particle size analyzer results

displayed in the Table 4.2 bellow.

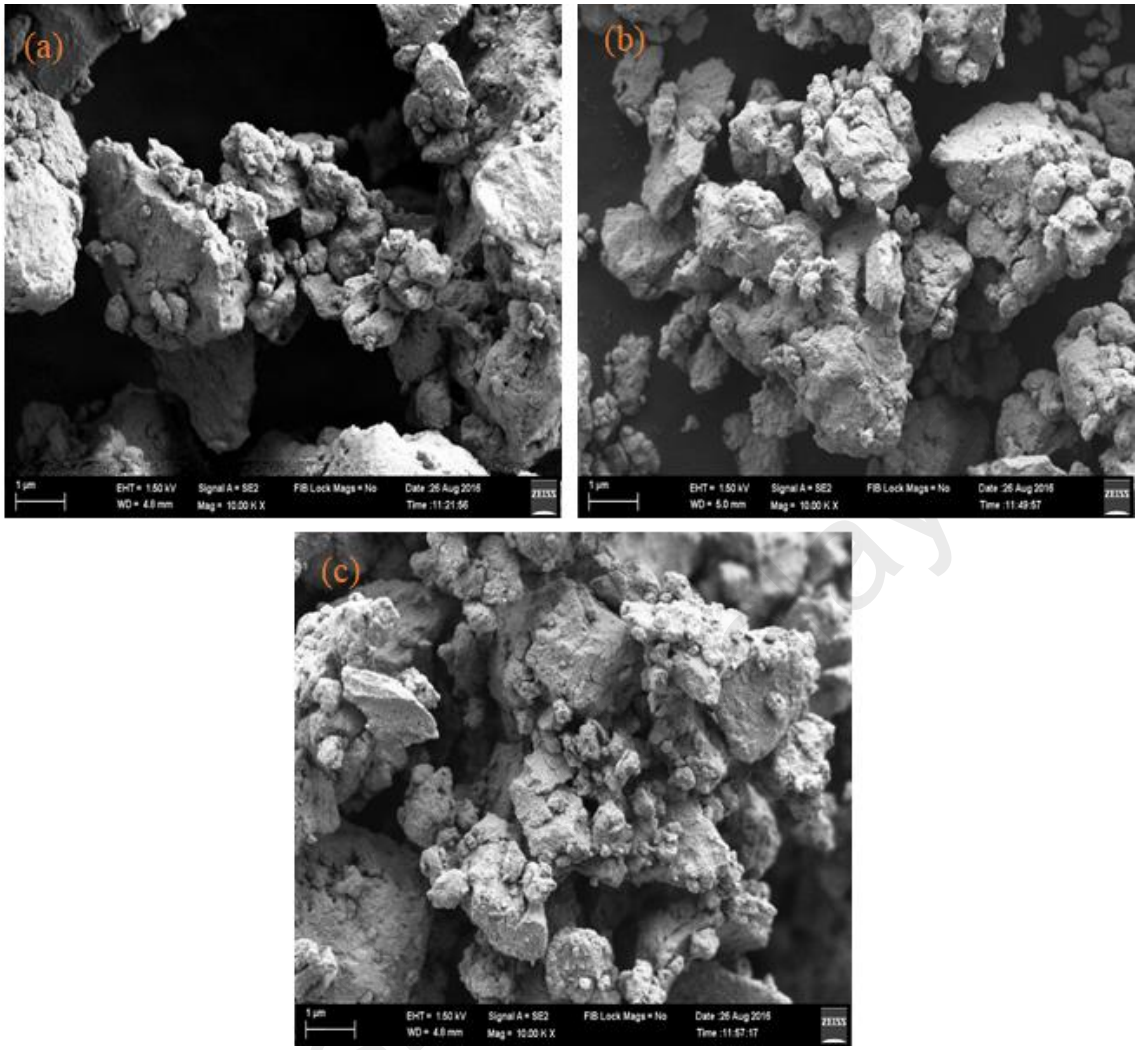

Figure 4.13: As milled powders' FESEM images with 10000 x magnification. (a), (b) and (c) represents 10 h, 15 h and 20 h ball milling samples respectively.

Table 4.2 Particle size via Particle size analyzer.

Ball milling duration	Particle size (μm)
10 h	16.2
15 h	9.7
20 h	11.2

The particle size in the table 4.2 provides information regarding average and standard deviation of particle size. Based on the raw data from the particle analyzer as shown below, the 20 h sample has the highest standard deviation as predicted above. We observe

the reduction of grain size from 10 h to 15 h then again increase in grain size. This phenomenon is due to the heat and energy generates for the longer ball milling hours.

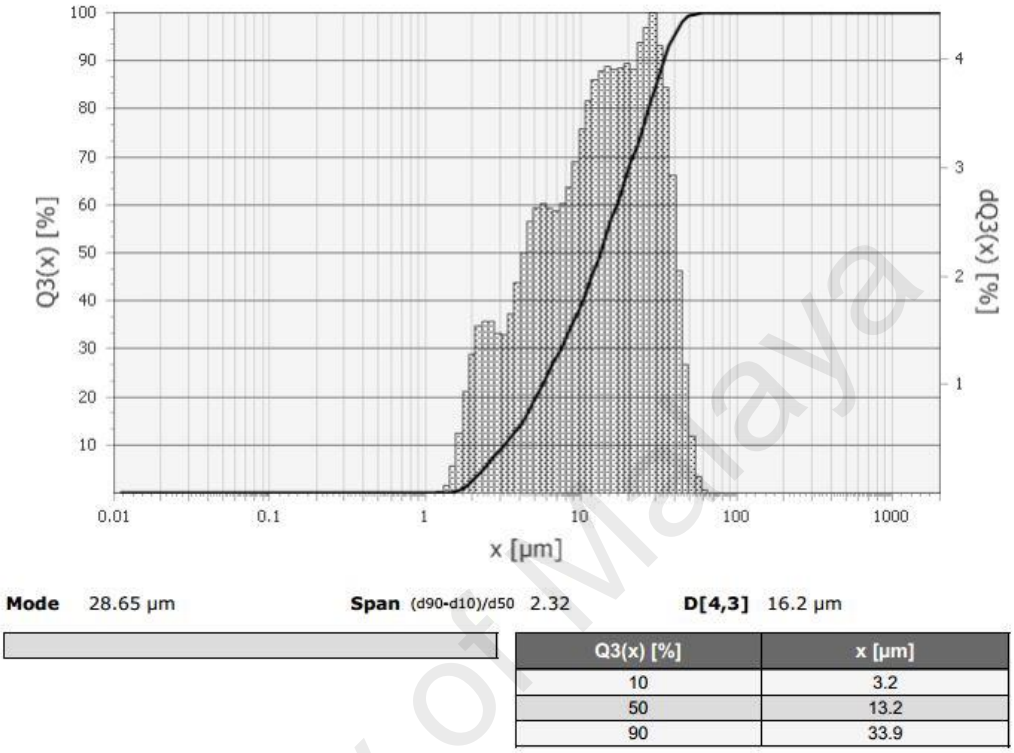

Q3(x) [%]	x [µm]
10	3.2
50	13.2
90	33.9

Figure 4.14: Particle size analyzer result for 10 h as milled $Bi_{0.6}FeCo_3Sb_{12}$ powder.

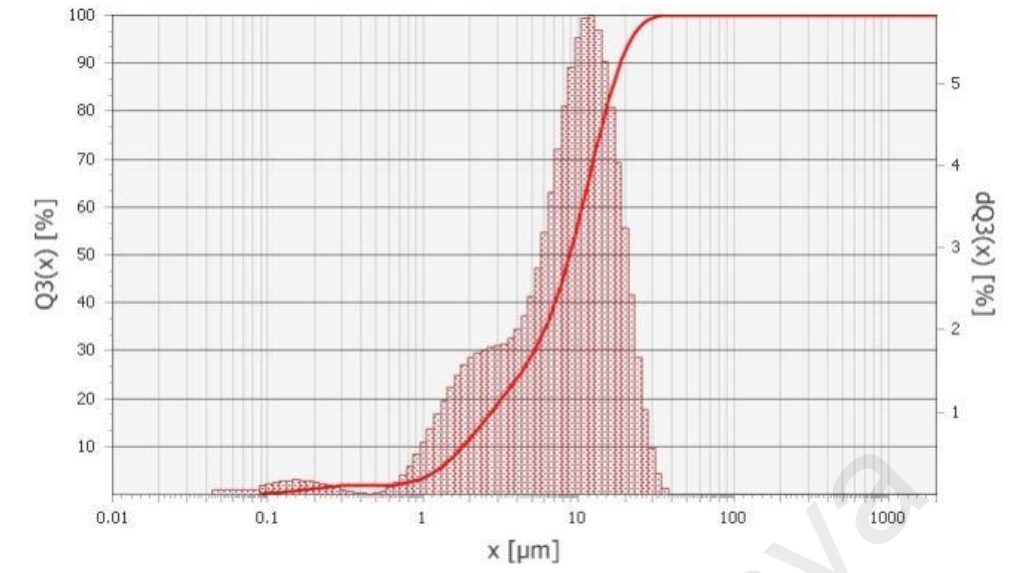

Q3(x) [%]	x [µm]
10	1.8
50	8.8
90	18.6

Figure 4.15: Particle size analyzer result for 15 h as milled $Bi_{0.6}FeCo_3Sb_{12}$ powder.

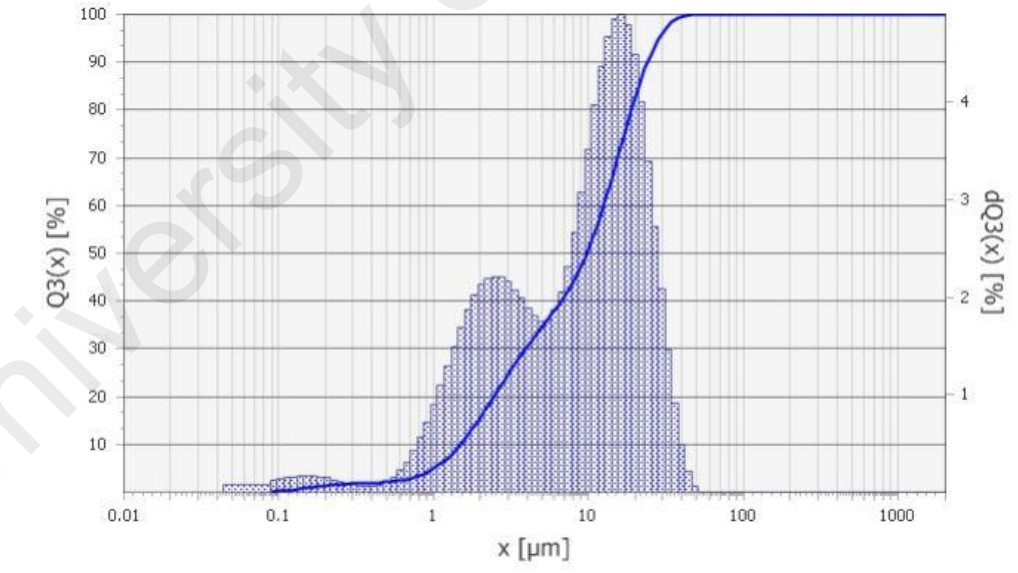

Q3(x) [%]	x [µm]
10	1.5
50	9.7
90	24

Figure 4.16: Particle size analyzer result for 20 h as milled $Bi_{0.6}FeCo_3Sb_{12}$ powder.

However, the distribution of particle size described so far does not correlate directly to the XRD pattern, as broadening of the XRD peak due to particle size is generally observed for particles in the range of 200nm, and is especially pronounced for particles <50nm. Therefore, it can leads to the conclusion of the following observations of the broader XRD patterns for the ball milled powder in Figure 4.16:

(1) The XRD patterns in Figure 4.16 show a more amorphous character compared to the XRD peaks of the SPSed samples shown in Figure 4.13, as they are not sintered, and are therefore broader.

(2) Broadening of the XRD peaks is caused by crystal lattice distortion (micro-strain) due to dislocations, which may be true for the ball milled samples which have been subjected to high mechanical stress.

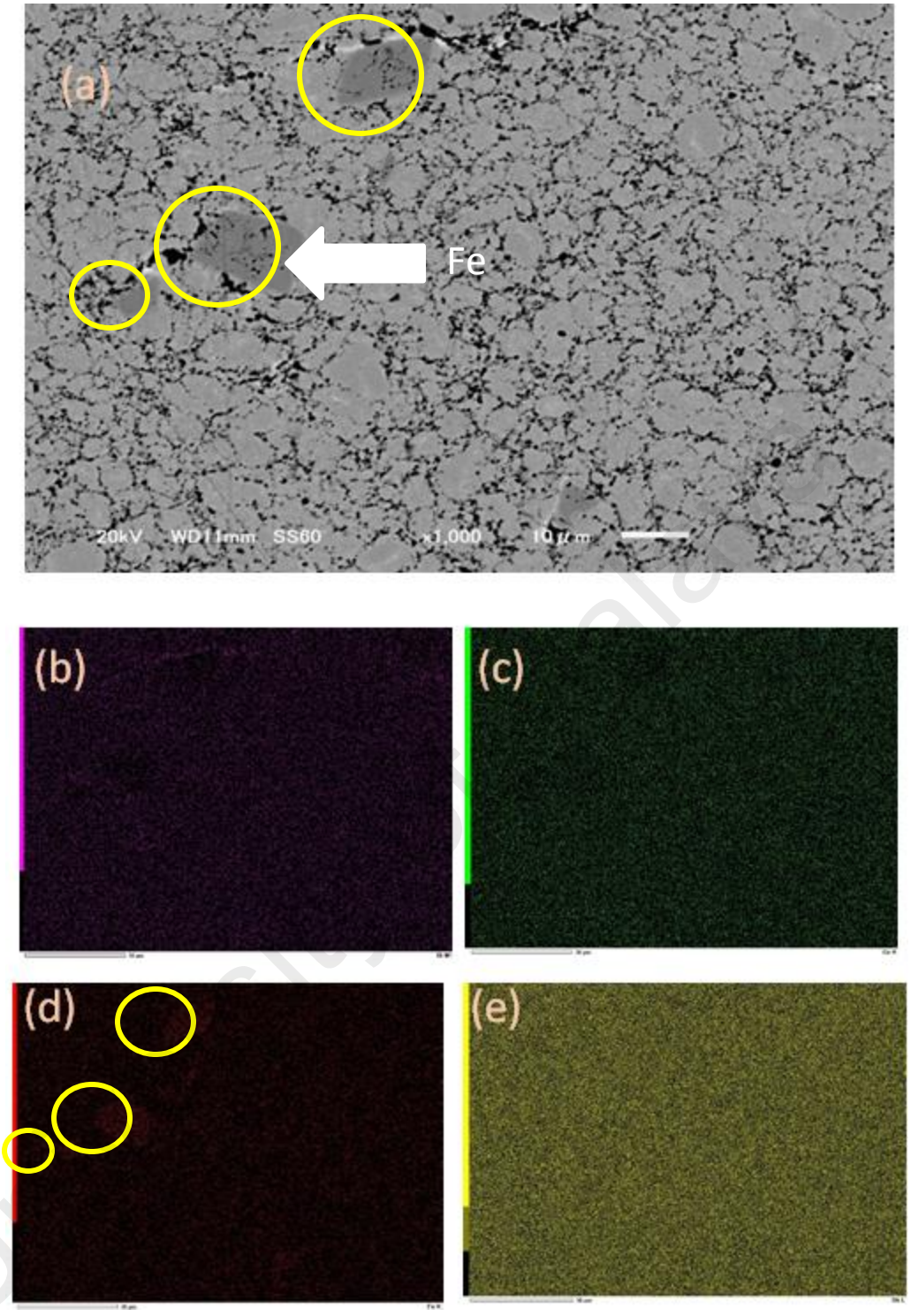

Figure 4.17: SEM images of $Bi_{0.6}FeCo_3Sb_{12}$ skutterudite after 10 h BM and SPS, (a) micrograph of an SPS-compacted sample, an elemental mapping of (b), (c), (d) and (e) show Bi, Co, Fe and Sb by EDS.

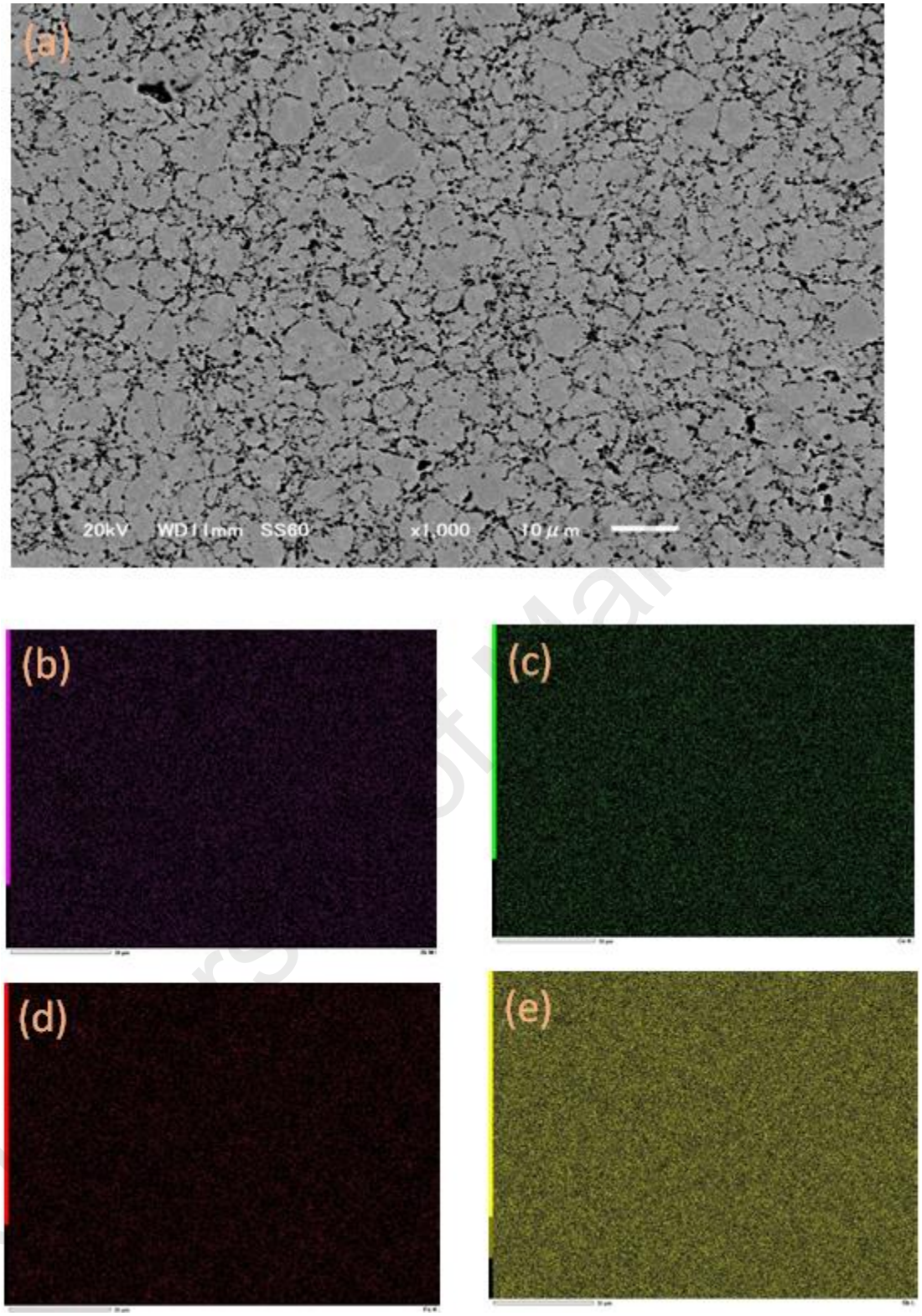

Figure 4.18: SEM images of $Bi_{0.6}FeCo_3Sb_{12}$ skutterudite after 15 h BM and SPS, (a) micrograph of an SPS-compacted sample, an elemental mapping of (b), (c), (d) and (e) show Bi, Co, Fe and Sb by EDS.

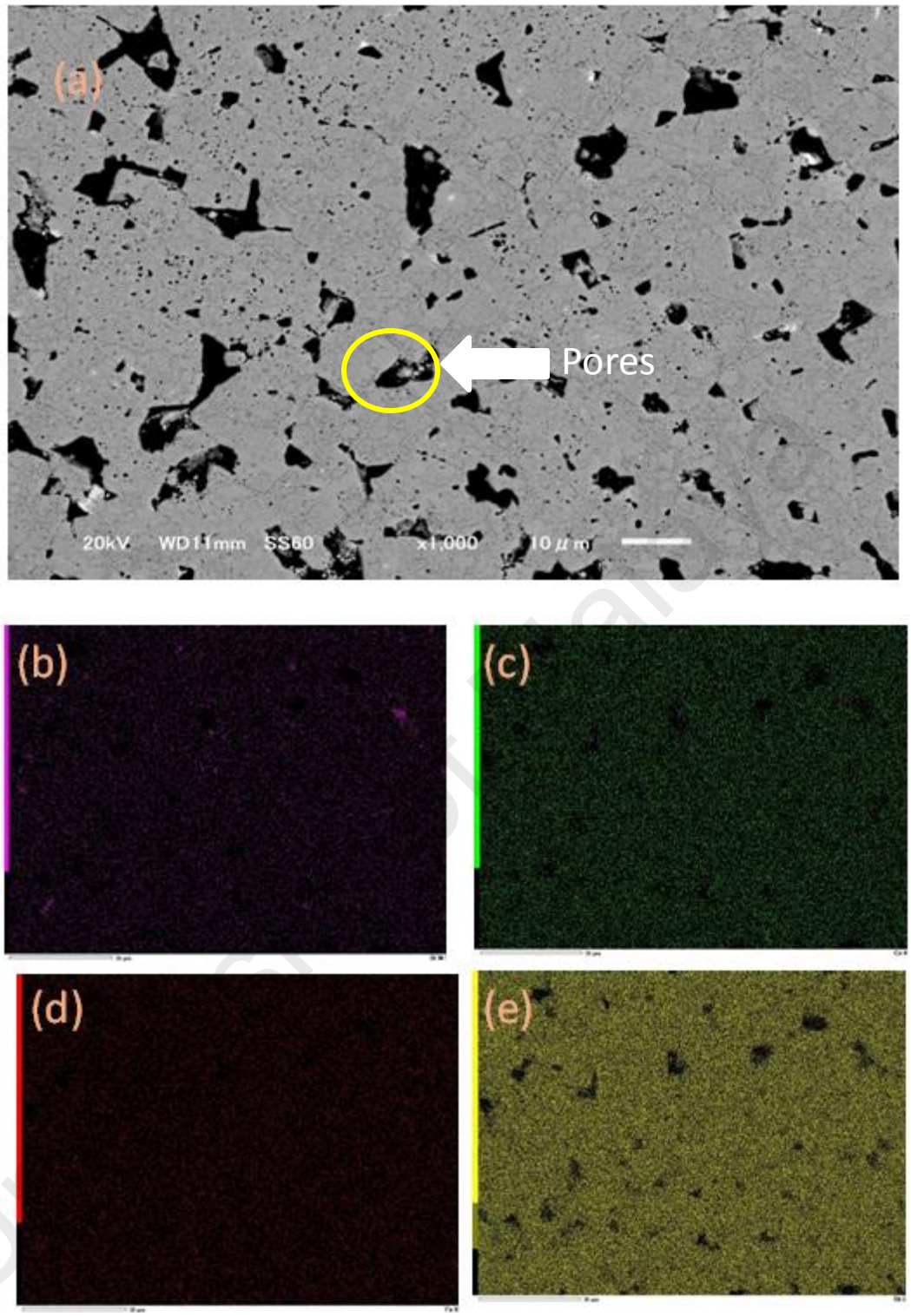

Figure 4.19: SEM images of $Bi_{0.6}FeCo_3Sb_{12}$ skutterudite after 20 h BM and SPS, (a) micrograph of an SPS-compacted sample, an elemental mapping of (b), (c), (d) and (e) show Bi, Co, Fe and Sb by EDS.

4.7 TE Property Investigation

At first as-milled $Bi_xFeCo_3Sb_{12}$ skutterudite (x=0.6) powder with different ball milling condition was sintered using SPS at 620^0C for 10 min under 50MPa. Due to melting of Bi in that condition the sintering condition was changed to 36 MPa for 10 min. In both case single phase skutterudite was able to form but the melting of Bi is less for the later one.

4.7.1 Seebeck coefficient

Figure 4.20 depicts the temperature dependences of Seebeck coefficient for $Bi_{0.6}FeCo_3Sb_{12}$ skutterudites for different milling conditions from 373 K to 673 K.

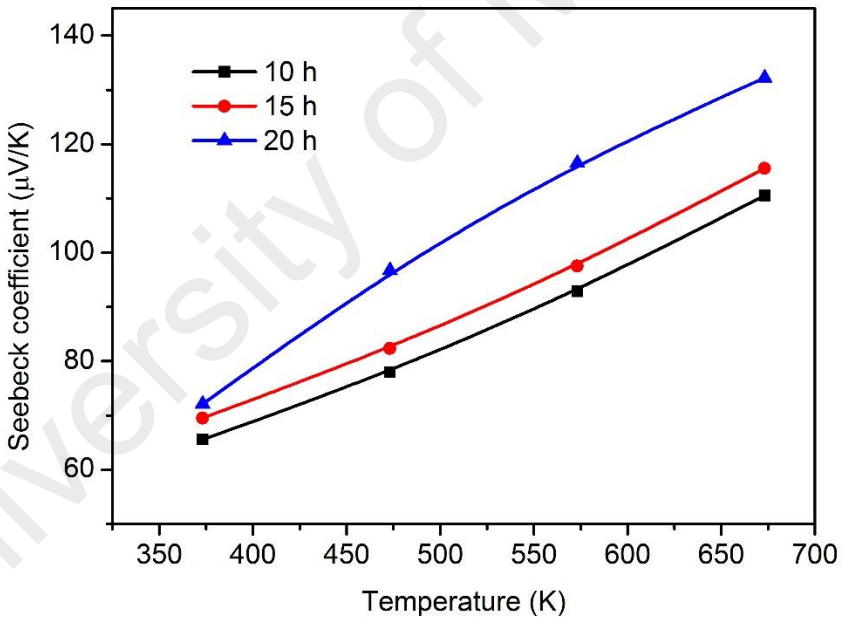

Figure 4.20: Temperature dependence of the Seebeck coefficient of $Bi_{0.6}FeCo_3Sb_{12}$ skutterudite for 10 h, 15 h and 20 h ball milling time.

All the samples have positive Seebeck coefficient indicating p-type conduction of these samples. According to the formula of thermoelectric figure of merit Seebeck coefficient is directly related to electrical conductivity and thermal conductivity. Seebeck coefficient tends to decrease when electrical conductivity increases, usually due to the

increase in carrier concentration upon doping. This behavior is observed in the figure 4.21 with comparison of the electrical conductivity in respect of the temperature. The seebeck coefficient increases gradually with temperature increment for every samples. Bismuth itself is an electron acceptor and therefore has the effect of producing a positive Seebeck coefficient for the Bi doped $FeCo_3Sb_{12}$ sample. In the 20 h BM sample, there are no Bi impurities, which result in a thermoelectric material which relies on holes as the dominant charge conductor. However, in the 10 h and 15 h samples, XRD suggest that Bi impurities exist. Bi itself has a negative Seebeck coefficient (-72 µV/K), which when they coexist in the bulk skutterudite result in a reduced Seebeck coefficients for the 10 h and 15 h sample.

4.7.2 Electrical conductivity

The electrical conductivity of $Bi_{0.6}FeCo_3Sb_{12}$ measured by ZEM-1 is shown in Figure 4.21, for all three samples with varying ball milling time.

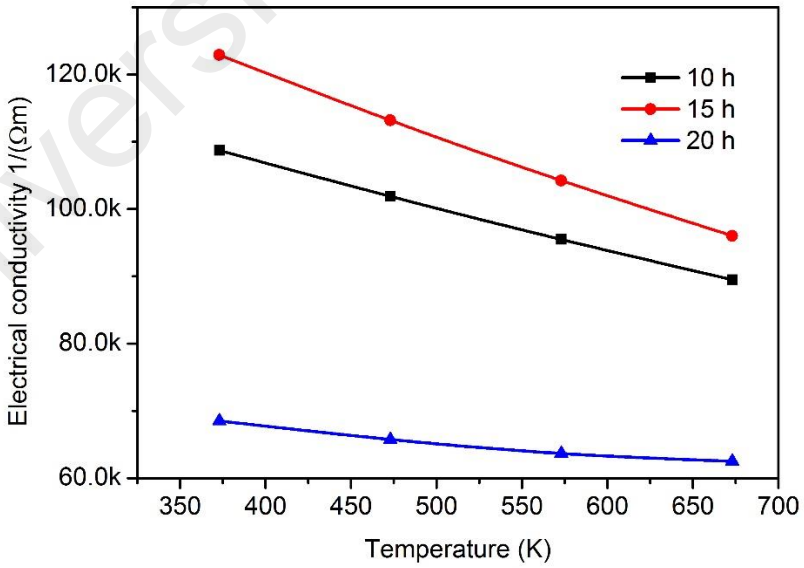

Figure 4.21: Temperature dependence of the electrical conductivities of $Bi_{0.6}FeCo_3Sb_{12}$ skutterudite for 10 h, 15 h and 20 h ball milling time.

The highest electrical conductivity was demonstrated by the 15 h milling sample, this is most probably due to the highly homogenous nature and small grain size of the resulting skutterudite. The 20 h milled samples showed the lowest electrical conductivity, due to the highly inhomogeneous nature of the sample, and its highly porous texture. The electrical conductivity of the samples are very high. The highest electrical conductivity was observed at 373 K of $122x10^3$ $\Omega^{-1}m^{-1}$ for 15 h MA-ed sample. The 15 h milled powders has given electrical conductivity of $122x10^3$ $\Omega^{-1}m^{-1}$ in comparison to the 400 $\Omega^{-1}m^{-1}$ Fe doped $CoSb_3$ skutterudite reported by Ur et al (Ur, Kwon, & Kim, 2007b). Tentatively, Bi doping shows improvement of the electrical conductivity over the original ternary skutterudite, $FeCoSb_3$. This is probably due to the fact that the Bi atom acts as an acceptor and improves the charge conduction due to holes. All the three samples given high density bulks. 10 h, 15 h and 20 h hour ball milled samples have 98%, 97% and 93% densities respectively. Even at the lowest value of electrical conduction property- all the 3 samples exhibits higher electrical conductivity compared to Bi added skutterudite reported by Mallik et al. ~ 34000 $\Omega^{-1}m^{-1}$ (Mallik et al., 2013). In this case, we expect that the dominant contribution to the electrical conductivity comes from the substitution of Fe into the $CoSb_3$ lattice. Since the occupancy of Fe in the resulting skutterudite is fairly constant, as indicated in Table 2, the electrical conductivity as a function of Fe is also constant, which implies that the variation in electrical conductivity for the three samples studied is largely due to the grain size in the bulk material. Therefore, the 15 h milled sample which has the smallest grain size has produced the sample with highest electrical conductivity.

4.7.3 Thermal conductivity

The reason of Fe substitution to binary $CoSb_3$ is to reduce thermal conductivity, get single phase skutterudite, and prevent phase decomposition and Sb evaporation (Ur et al., 2007b). Fe substitution reduced thermal conductivity and Bi addition is to improve ZT. From the Figure 4.22 showing the total thermal conductivity of the samples it has shown that 20 h samples has the lowest thermal conductivity and 10 h has the highest.

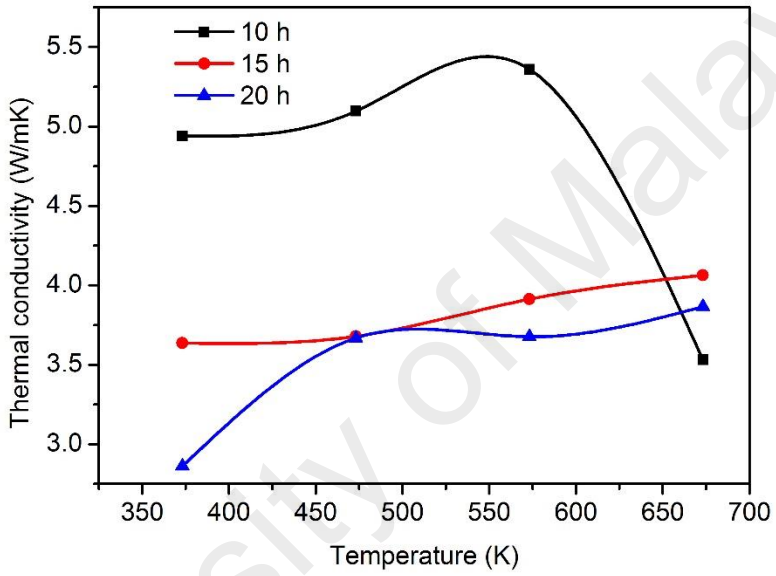

Figure 4.22: Temperature dependence of the total thermal conductivity of $Bi_{0.6}FeCo_3Sb_{12}$ skutterudite for 10 h, 15 h and 20 h ball milling time.

From the SEM image in Figure 8(a) it can be observed that this 20 h sample is porous. The low thermal conductivity of the 20 h has the lowest thermal conductivity due to the porous nature of the sample.

In comparison, the 10 h has the highest thermal conductivity due to the agglomerated Fe which causes heat to dissipate easier in these domains. Comparison of the thermal conductivity with the binary $CoSb_3$, it is confirmed that the Bi addition and Fe substitution lowered the thermal conductivity. The total thermal conductivity is the sum of both lattice

and charge carriers contribution of heat. Because both phonons and electrons are carriers of heat in the solid samples. Total thermal conductivity can be represented by this formula

$$K_{Total} = K_e + K_L \tag{4.1}$$

By Wiedemann-Franz law carrier contribution can be calculated

$$K_e = L_0 \sigma T \tag{4.2}$$

Where σ is the electrical conductivity and L_0 is the Lorenz number = 2.45 x 10^{-8} V^2K^{-2}. K_L was calculated by subtracting K_e from the total thermal conductivity. The plots for total thermal conductivity, electron thermal conductivity and lattice thermal conductivity are shown in Figure 4.22, Figure 4.23 (a) and (b) respectively. In the 15 h sample the lattice thermal conductivity does not vary largely. For all the samples electronic contribution K_e displayed at Figure 4.23 (a) increases with the increment of the temperature. In Figure 4.23 (b) the lattice contribution K_L into the total thermal conductivity very close in magnitude to the total thermal conductivity graph. Thus, the main contributing factor to the overall thermal conductivity is the lattice thermal conductivity. In this case, Bi addition plays the primary role, as a filler in the skutterudite void, which serves to attenuate the thermal conductivity. This can be supported by the comparison between the 10 h sample and 15 h sample, which contains 28% and 46% Bi, respectively, as obtained by Rietveld analysis.

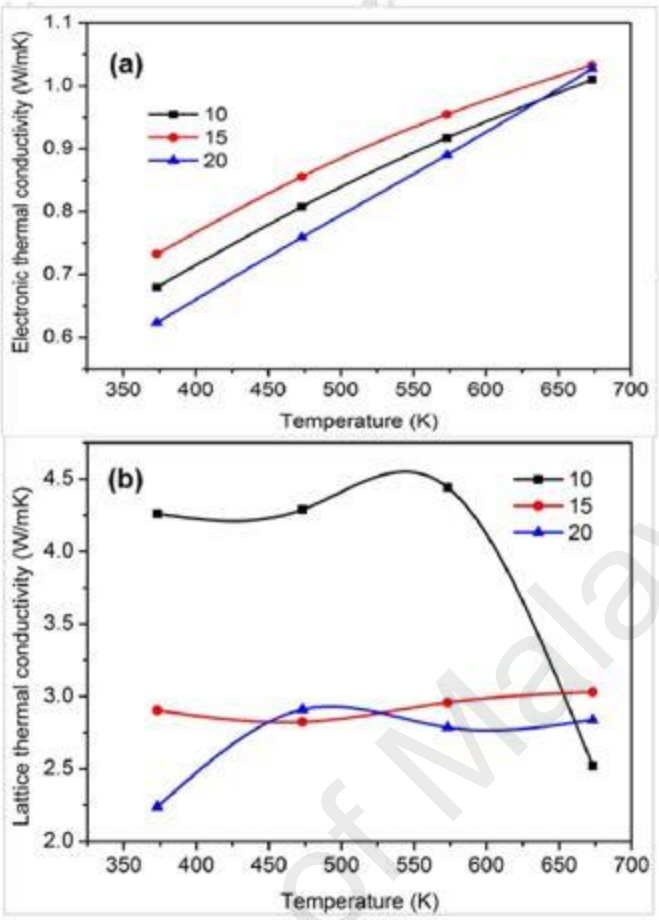

Figure 4.23: (a) Temperature dependence of electronic thermal conductivity and (b) Lattice thermal conductivity of 10 h, 15 h and 20 h ball milled $Bi_{0.6}FeCo_3Sb_{12}$ skutterudite samples.

The 15 h sample possesses the lower thermal conductivity due to the higher proportion of Bi filler. The role of the Bi filler to reduce thermal conductivity of the skutterudite samples in comparison with the binary $CoSb_3$, has also been proven by Ur et al (Ur et al., 2007b), who demonstrated that Fe substitution $CoSb_3$ has distinctively lowered thermal conductivity compared to binary $CoSb_3$, and Mallik et al (Mallik et al., 2013) have shown that the addition of Bi has resulted to reduce the thermal conductivity compared to binary $CoSb_3$.

4.7.4 Figure of Merit ZT

ZT is calculated in terms of electrical resistivity, Seebeck and thermal conductivity. The results of 10 h, 15 h and 20 h ball milled samples are shown in Figure 4.24.

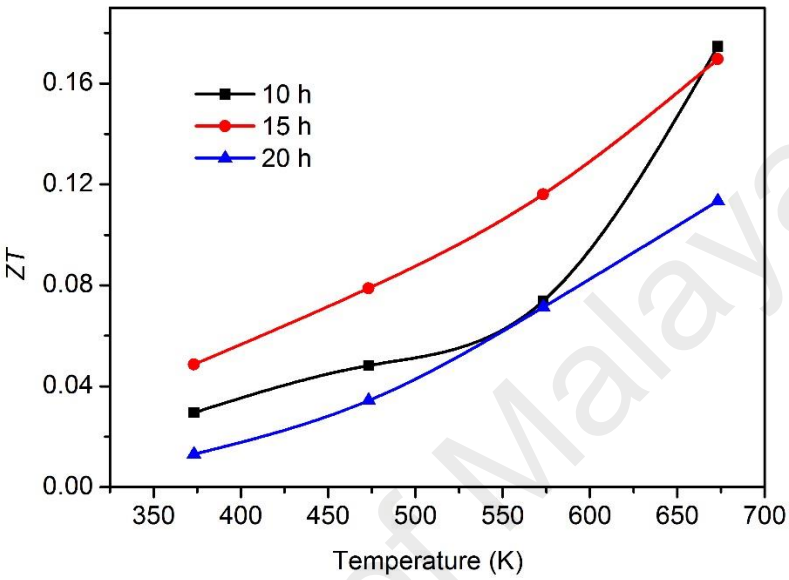

Figure 4.24: Temperature dependence of the dimensionless Figure of merit ZT for 10 h 15 h and 20 h ball milled $Bi_{0.6}FeCo_3Sb_{12}$ skutterudite samples.

Also a comparison table (Table No. 4.3) of individual results of thermoelectric properties of binary and ternary skutterudite is presented for comparative analysis.

Table 4.3: Comparison among the 10 h, 15 h and 20 h ball milled and SPS samples with binary, Fe doped ternary and Bi added Co4Sb12 skutterudite at 600 K.

Thermoelectric properties	**10 h**	**15 h**	**20 h**	**$FeCo_4Sb_4$ (Ur et al., 2007b)**	**$Bi_xCo_4Sb_{12}$ (x=0.5) (Mallik et al., 2013)**	**$CoSb_3$ (Ur et al., 2007b)**
Electrical Conductivity ($S.m^{-1}$)	~97000	~100001	~64000	~40000	~27500	~18200
Seebeck Coefficient (μV/K)	~97	~102	~121	~105	~190	~200
Thermal conductivity (W/mK)	~4.87	~3.95	~3.73	~4.9	~1.65	~5
$ZT_{(Max)}$	0.18	0.17	0.11	0.12	0.51	0.08

From the above analysis, we first consider the individual contributions of the electrical conductivity, Seebeck coefficient and thermal conductivity in comparison to related binary and ternary skutterudite formulations gathered from the Table 1.1 and in comparison with Mallik et al. (Mallik et al., 2013) . It can be seen that the maximum electrical conductivity of the quaternary formulation $Bi_{0.6}FeCoSb_{12}$ (at 673 K) is 2.74 times higher than the $Bi_{0.5}Co_4Sb_{12}$ (at 750 K) formulation reported by Malik et al (Mallik et al., 2013) which has the maximum electrical conductivity in terms of magnitude comparing with the other reported formulations by Mallik and co-authors. For the Seebeck coefficient, quaternary mixture is slightly lower than or almost similar to the values of the different filling level of Bi reported by Malik et al (Mallik et al., 2013), whilst the thermal conductivity of the quaternary mixture is comparable to $Bi_xCo_4Sb_{12}$ formulations. In addition, the 20 h sample demonstrated some porosity which further reduced the thermal conductivity, thus illustrating a further pathway of MA processing which may improve the ZT through introduction of porosity. However, since $ZT= S^2T/\sigma K$ it can be seen that the S^2 term dominates the ZT, the overall quaternary formulation ends up being lower ZT due to the fact Seebeck is low. But in comparison with the ternary $FeCo_3Sb_{12}$ (Ur et al., 2007b) and $Bi_xCo_4Sb_{12}$ formulations (except x = 0.5) (Mallik et al., 2013) the ZT of $Bi_{0.6}FeCo_3Sb_{12}$ is 0.18 at 673 K for 10 h and 0.17 at 673 K for 15 h ball milling time. These are higher than the compared ternary skutterudite systems. This work is still, useful in identifying the electronic contributions of the Bi dopant to the Fe, Co Sb mixture to improve the electrical conductivity, and also the identification of the optimal MA alloying parameters that will produce a homogenous microstructure needed for good TE performance. In particular, we can see that the milling time has an impact on the particle size, and hence the extent of Bi filling into the skutterudite lattice during the SPS process, as demonstrated by a lower proportion of Bi filling for low milling times (10 h). Thus, the milling time does not only affect the physical dimensions of the skutterudite

morphology, but is also able to influence the actual composition of the resulting skutterudite. The 10 h sample shows the highest ZT = 0.18 amongst these three samples, whilst the 15 h sample (ZT=0.17) comes with a magnitude of ZT which is close to 10 h sample, implying that the agglomeration that resulted in the 20 h sample (ZT=0.11) is detrimental to thermoelectric performance.

CHAPTER 5: CONCLUSION

5.1 Conclusion

The study of Bi filling with $FeCo_3Sb_{12}$ is a new composition in the search of high ZT thermoelectric materials. To date, no one has reported this composition with Bi filling. The study of a new formulation, $Bi_{0.6}FeCo_3Sb_{12}$ was proposed to achieve simultaneous filling of Bi in the Co_4Sb_{12} skutterudite, with substitution of Fe in Co sites. This strategy succeeded in simultaneously increasing the electrical conductivity and decreasing the thermal conductivity, and is thus a useful strategy for future design of skutterudite materials for thermoelectrics. Our analysis of the effect of the ball milling conditions on the thermoelectric performance of this formulations also gives insight to the optimal conditions which may yield a good microstructure, and hence good thermoelectric performance. It has been shown that moderate milling times will provide a well distributed sample which is conducive for good electrical conductivity and low thermal conductivity. We have also demonstrated that milling time is able to affect the final composition of the skutterudite in terms of the amount of Bi filling, despite using the same nominal composition for all three samples. For this work we have successfully achieved our objectives. To be specific Synthesis of $Bi_{0.6}FeCo_3Sb_{12}$ skutterudites for high efficiency thermoelectric properties has been successfully achieved. The effect of ball milling parameter was studied and for $Bi_{0.6}FeCo_3Sb_{12}$ quaternary single phase skuttterudite formulation. For ball milling study, 15 h ball milling time was optimized and proposed. The particle size on thermoelectric properties of $Bi_{0.6}FeCo_3Sb_{12}$ was studied. Benefits of homogenous particle distribution has shown and also the effect of conglomerated particles has been discussed. Lastly, filling level of Bi on the $FeCo_3Sb_{12}$ skutterudite for different milling duration has been studied. This work is useful in providing a direct correlation between BM process parameters and the resulting

microstructure and thermoelectric characteristics, thus providing a design pathway to improve thermoelectric parameters of skutterudites as a function of BM parameters.

5.2 Future Work

Future work for this formulation is to further study to improve the thermoelectric properties for this formulation. On the other hand more comparison with the filling level of Bi need to be studied. Here, following points are suggested for future work.

- Study filling level for the formulation $Bi_xFeCo_3Sb_{12}$ (x = 0.2, 0.4, 0.8) to further compare and optimize the filling level of Bi.
- Investigate with another filler with this $Bi_xY_bFeCo_3Sb_{12}$ formulation. Supposedly Indium (Y= In) to increase the overall ZT and study the effect of another filler on the microstructure and overall thermoelectric performance.

REFERENCES

Alam, H., & Ramakrishna, S. (2013). A review on the enhancement of figure of merit from bulk to nano-thermoelectric materials. *Nano Energy, 2*(2), 190-212.

Arita, Y., Ogawa, T., Kobayashi, H., Iwasaki, K., Matsui, T., & Nagasaki, T. (2005). Thermoelectric properties of uranium filled skutterudites Uy (FexCo4− x) Sb12. *Journal of nuclear materials, 344*(1-3), 79-83.

Bai, S., Pei, Y., Chen, L., Zhang, W., Zhao, X., & Yang, J. (2009). Enhanced thermoelectric performance of dual-element-filled skutterudites BaxCeyCo4Sb12. *Acta Materialia, 57*(11), 3135-3139.

Ballikaya, S., Uzar, N., Yildirim, S., Salvador, J. R., & Uher, C. (2012). High thermoelectric performance of In, Yb, Ce multiple filled CoSb3 based skutterudite compounds. *Journal of solid state chemistry, 193*, 31-35.

Bao, S., Yang, J., Peng, J., Zhu, W., Fan, X. a., & Song, X. (2006). Preparation and thermoelectric properties of LaxFeCo3Sb12 skutterudites by mechanical alloying and hot pressing. *Journal of Alloys and Compounds, 421*(1-2), 105-108.

Bao, S., Yang, J., Zhu, W., Fan, X. a., Duan, X., & Peng, J. (2006). Preparation and thermoelectric properties of La filled skutterudites by mechanical alloying and hot pressing. *Materials Letters, 60*(16), 2029-2032.

Benjamin, J., & Volin, T. (1974). The mechanism of mechanical alloying. *Metallurgical transactions, 5*(8), 1929-1934.

Benjamin, J. S. (1970). Dispersion strengthened superalloys by mechanical alloying. *Metallurgical transactions, 1*(10), 2943-2951.

Bux, S. K., Fleurial, J.-P., & Kaner, R. B. (2010). Nanostructured materials for thermoelectric applications. *Chemical Communications, 46*(44), 8311-8324.

Chen, D., Ni, S., & Chen, Z. (2007). Synthesis of Fe3O4 nanoparticles by wet milling iron powder in a planetary ball mill. *China Particuology, 5*(5), 357-358. doi: http://dx.doi.org/10.1016/j.cpart.2007.05.005

Chen, G., Kraemer, D., Muto, A., McEnaney, K., Feng, H.-P., Liu, W.-S., . . . Ren, Z. (2011). *Thermoelectric energy conversion using nanostructured materials.* Paper presented at the SPIE Defense, Security, and Sensing.

Dmitriev, A. V., & Zvyagin, I. P. (2010). Current trends in the physics of thermoelectric materials. *Physics-Uspekhi, 53*(8), 789-803.

Dughaish, Z. (2002). Lead telluride as a thermoelectric material for thermoelectric power generation. *Physica B: Condensed Matter, 322*(1), 205-223.

El-Eskandarany, M. S., Aoki, K., Itoh, H., & Suzuki, K. (1991). Effect of ball-to-powder weight ratio on the amorphization reaction of Al 50 Ta 50 by ball milling. *Journal of the Less Common Metals, 169*(2), 235-244.

Froes, F. (1990). The structural applications of mechanical alloying. *JOM Journal of the Minerals, Metals and Materials Society, 42*(12), 24-25.

Gilman, P., & Benjamin, J. (1983). Mechanical alloying. *Annual Review of Materials Science, 13*(1), 279-300.

Harnwunggmoung, A., Kurosaki, K., Ohishi, Y., Muta, H., & Yamanaka, S. (2011). Effects of Tl-filling into the voids and Rh substitution for Co on the thermoelectric properties of CoSb3. *Journal of Alloys and Compounds, 509*(3), 1084-1089.

Harringa, J., Cook, B., & Beaudry, B. (1992). Effects of vial shape on the rate of mechanical alloying in Si80Ge20. *Journal of materials science, 27*(3), 801-804.

Hicks, L., & Dresselhaus, M. S. (1993). Effect of quantum-well structures on the thermoelectric figure of merit. *Physical Review B, 47*(19), 12727.

Hmood, A., Kadhim, A., & Hassan, H. A. (2013). Fabrication and characterization of Pb1− xYbxTe-based alloy thin-film thermoelectric generators grown by thermal evaporation technique. *Materials Science in Semiconductor Processing, 16*(3), 612-618.

Hochbaum, A. I., Chen, R., Delgado, R. D., Liang, W., Garnett, E. C., Najarian, M., . . . Yang, P. (2008). Enhanced thermoelectric performance of rough silicon nanowires. *Nature, 451*(7175), 163-167.

Jiang, Y., Jia, X., Su, T., Dong, N., Yu, F., Tian, Y., . . . Ma, H. (2010). Thermoelectric properties of SmxCo4Sb12 prepared by high pressure and high temperature. *Journal of Alloys and Compounds, 493*(1-2), 535-538.

Jie, Q., Wang, H., Liu, W., Wang, H., Chen, G., & Ren, Z. (2013). Fast phase formation of double-filled p-type skutterudites by ball-milling and hot-pressing. *Physical Chemistry Chemical Physics, 15*(18), 6809-6816.

Jung, J.-Y., Hong, S.-J., You, S.-W., Jeong, Y.-J., Lee, J.-I., Ur, S.-C., & Kim, I.-H. (2007). *Thermoelectric properties of In z Co 4 Sb 12-y Te y skutterudites.* Paper presented at the Thermoelectrics, 2007. ICT 2007. 26th International Conference on.

Kalkan, N., Young, E., & Celiktas, A. (2012). Solar thermal air conditioning technology reducing the footprint of solar thermal air conditioning. *Renewable and Sustainable Energy Reviews, 16*(8), 6352-6383.

Kawamoto, H. (2009). R&D trends in high efficiency thermoelectric conversion materials for waste heat recovery: NISTEP Science & Technology Foresight Center.

Keskar, G., Iyyamperumal, E., Hitchcock, D. A., He, J., Rao, A. M., & Pfefferle, L. D. (2012). Significant improvement of thermoelectric performance in nanostructured bismuth networks. *Nano Energy, 1*(5), 706-713.

Kishi, M., Nemoto, H., Hamao, T., Yamamoto, M., Sudou, S., Mandai, M., & Yamamoto, S. (1999). *Micro thermoelectric modules and their application to wristwatches as*

an energy source. Paper presented at the Thermoelectrics, 1999. Eighteenth International Conference on.

Kiyoshi, I. (1970). Servocontrol system for discharge sintering: Google Patents.

Koch, C. (1993). The synthesis and structure of nanocrystalline materials produced by mechanical attrition: a review. *Nanostructured materials, 2*(2), 109-129.

Spark Plasma Sintering

Lab, L. L. N. (2017). Estimated U.S Energy Consumption in 2017 : 97.7 Quads.

Lee, P.-Y., Yang, J.-L., & Lin, H.-M. (1998). Amorphization behaviour in mechanically alloyed Ni—Ta powders. *Journal of materials science, 33*(1), 235-239.

Lee, P., & Koch, C. (1988). Formation of amorphous Ni-Zr alloy powder by mechanical alloying of intermetallic powder mixtures and mixtures of nickel or zirconium with intermetallics. *Journal of materials science, 23*(8), 2837-2845.

Lee, W., & Kwun, S. (1996). The effects of process control agents on mechanical alloying mechanisms in the Ti • Al system. *Journal of Alloys and Compounds, 240*(1), 193-199.

Li, J.-F., Liu, W.-S., Zhao, L.-D., & Zhou, M. (2010). High-performance nanostructured thermoelectric materials. *NPG Asia Materials, 2*(4), 152-158.

Liu, K., Dong, X., & Jiuxing, Z. (2006). The effects of La on thermoelectric properties of La x Co 4 Sb 12 prepared by MA–SPS. *Materials chemistry and physics, 96*(2), 371-375.

Liu, W., Yan, X., Chen, G., & Ren, Z. (2012). Recent advances in thermoelectric nanocomposites. *Nano Energy, 1*(1), 42-56.

Lu, P.-X., Wu, F., Han, H.-L., Wang, Q., Shen, Z.-G., & Hu, X. (2010). Thermoelectric properties of rare earths filled CoSb3 based nanostructure skutterudite. *Journal of Alloys and Compounds, 505*(1), 255-258.

Mallik, R., Anbalagan, R., Raut, K., Bali, A., Royanian, E., Bauer, E., . . . Rogl, P. (2013). Thermoelectric properties of Bi-added Co4Sb12 skutterudites. *Journal of Physics: Condensed Matter, 25*(10), 105701.

Munir, Z., Anselmi-Tamburini, U., & Ohyanagi, M. (2006). The effect of electric field and pressure on the synthesis and consolidation of materials: a review of the spark plasma sintering method. *Journal of materials science, 41*(3), 763-777.

Nie, G., Ochi, T., Suzuki, S., Kikuchi, M., Ito, S., & Guo, J. (2014). Stability of skutterudite thermoelectric materials. *Journal of Electronic Materials, 43*(6), 1752-1756.

Nolas, G., Morelli, D., & Tritt, T. M. (1999). Skutterudites: A phonon-glass-electron crystal approach to advanced thermoelectric energy conversion applications. *Annual Review of Materials Science, 29*(1), 89-116.

Nolas, G., Slack, G., Morelli, D., Tritt, T., & Ehrlich, A. (1996). The effect of rare-earth filling on the lattice thermal conductivity of skutterudites. *Journal of Applied Physics, 79*(8), 4002-4008.

Prometeon. Waste Heat to Electricity. In P. C. E. Technologies (Ed.).

Rodgers, P. (2008). Nanomaterials: Silicon goes thermoelectric. *Nature nanotechnology, 3*(2), 76-76.

Rogl, G., Grytsiv, A., Bauer, E., Rogl, P., & Zehetbauer, M. (2010). Thermoelectric properties of novel skutterudites with didymium: DD y (Fe 1− x Co x) 4 Sb 12 and DD y (Fe 1− x Ni x) 4 Sb 12. *Intermetallics, 18*(1), 57-64.

Rogl, G., Grytsiv, A., Rogl, P., Peranio, N., Bauer, E., Zehetbauer, M., & Eibl, O. (2014). n-Type skutterudites (R, Ba, Yb) yCo 4 Sb 12 (R= Sr, La, Mm, DD, SrMm, SrDD) approaching ZT≈ 2.0. *Acta Materialia, 63*, 30-43.

Rubi, C. S., Gowthaman, S., & Renganathan, N. Role of nanostructured materials in recent developments of thermoelectric nanocomposites.

Ryu, S., Kim, S., Kim, Y. D., & Moon, I. H. (2003). *Amorphization of Immiscible W-Cu-Pb System by Mechanical Alloying at Low Temperature.* Paper presented at the Journal of Metastable and Nanocrystalline Materials.

Said, S. M., Bashir, M. B. A., Sabri, M. F. M., Miyazaki, Y., Shnawah, D. A. A., Hakeem, A. S., . . . Elsheikh, M. H. (2017). Enhancement of Thermoelectric Behavior of La0. 5Co4Sb12− xTex Skutterudite Materials. *Metallurgical and Materials Transactions A, 48*(6), 3073-3081.

Schnelle, W., Leithe-Jasper, A., Rosner, H., Cardoso-Gil, R., Gumeniuk, R., Trots, D., . . . Grin, Y. (2008). Magnetic, thermal, and electronic properties of iron-antimony filled skutterudites M Fe 4 Sb 12 (M= Na, K, Ca, Sr, Ba, La, Yb). *Physical Review B, 77*(9), 094421.

Shi, X., Yang, J., Salvador, J. R., Chi, M., Cho, J. Y., Wang, H., . . . Chen, L. (2011). Multiple-filled skutterudites: high thermoelectric figure of merit through separately optimizing electrical and thermal transports. *Journal of the American Chemical Society, 133*(20), 7837-7846.

Snyder, G. J., & Toberer, E. S. (2008). Complex thermoelectric materials. *Nature materials, 7*(2), 105-114.

Sootsman, J. R., Chung, D. Y., & Kanatzidis, M. G. (2009). New and old concepts in thermoelectric materials. *Angewandte Chemie International Edition, 48*(46), 8616-8639.

Stordeur, M., & Rowe, D. (1995). CRC Handbook of Thermoelectrics. *CRC Press, Boca Raton, FL*, 251.

Suryanarayana, C. (2001). Mechanical alloying and milling. *Progress in materials science, 46*(1), 1-184.

Takacs, L., & Pardavi-Horvath, M. (1994). Nanocomposite formation in the Fe3O4-Zn system by reaction milling. *Journal of Applied Physics, 75*(10), 5864-5866.

Tang, G., Zhang, D., Chen, G., Xu, F., & Wang, Z. (2012). Thermoelectric properties in double-filled skutterudites InxNdyCo4Sb12. *Solid State Communications, 152*(24), 2193-2196.

Taoxiang, L., Xinfeng, T., Wenjie, X., Yonggao, Y., & Qingjie, Z. (2007). Crystal Structures and Thermoelectric Properties of Sm-Filled Skutterudite Compounds Smy Fex Co4-x Sb12. *Journal of Rare Earths, 25*(6), 739-743.

Tomeš, P., Trottmann, M., Suter, C., Aguirre, M. H., Steinfeld, A., Haueter, P., & Weidenkaff, A. (2010). Thermoelectric oxide modules (TOMs) for the direct conversion of simulated solar radiation into electrical energy. *Materials, 3*(4), 2801-2814.

Truong, D. N., Kleinke, H., & Gascoin, F. (2014). Thermoelectric properties of higher manganese silicide/multi-walled carbon nanotube composites. *Dalton Transactions, 43*(40), 15092-15097.

Ur, S.-C., Kwon, J.-C., & Kim, I.-H. (2007a). Thermoelectric properties of Fe-doped CoSb3 prepared by mechanical alloying and vacuum hot pressing. *Journal of Alloys and Compounds, 442*(1-2), 358-361.

Ur, S.-C., Kwon, J.-C., & Kim, I.-H. (2007b). Thermoelectric properties of Fe-doped CoSb 3 prepared by mechanical alloying and vacuum hot pressing. *Journal of Alloys and Compounds, 442*(1), 358-361.

Venkatasubramanian, R., Siivola, E., Colpitts, T., & O'quinn, B. (2001). Thin-film thermoelectric devices with high room-temperature figures of merit. *Nature, 413*(6856), 597-602.

Vineis, C. J., Shakouri, A., Majumdar, A., & Kanatzidis, M. G. (2010). Nanostructured thermoelectrics: big efficiency gains from small features. *Advanced Materials, 22*(36), 3970-3980.

Wang, T., Zhang, Y., Peng, Z., & Shu, G. (2011). A review of researches on thermal exhaust heat recovery with Rankine cycle. *Renewable and Sustainable Energy Reviews, 15*(6), 2862-2871.

Wang, X., Lee, H., Lan, Y., Zhu, G., Joshi, G., Wang, D., . . . Klatsky, J. (2008). Enhanced thermoelectric figure of merit in nanostructured n-type silicon germanium bulk alloy. *Applied Physics Letters, 93*(19), 193121.

Wei, J., Zhang, F., & Zhang, J. (2014). Effects of Cu doping on electronic structure and electrical transport properties of ZnO oxide. *Chinsese Journal of Quantum Electronics (量子电子学报), 31*(3), 372-378.

Yamada, K., & Koch, C. C. (1993). The influence of mill energy and temperature on the structure of the TiNi intermetallic after mechanical attrition. *Journal of materials research, 8*(06), 1317-1326.

Yan, X. (2010). *Thermoelectric Property Studies of Nanostructured Bulk Half-Heuslers and Bismuth Tellurides.* Boston College. Graduate School of Arts and Sciences.

Yang, J., Chen, Y., Peng, J., Song, X., Zhu, W., Su, J., & Chen, R. (2004). Synthesis of CoSb3 skutterudite by mechanical alloying. *Journal of Alloys and Compounds, 375*(1–2), 229-232. doi: http://dx.doi.org/10.1016/j.jallcom.2003.11.036

Yang, J., Xu, B., Zhang, L., Liu, Y., Yu, D., Liu, Z., . . . Tian, Y. (2013). Gadolinium filled CoSb3: High pressure synthesis and thermoelectric properties. *Materials Letters, 98*, 171-173.

Yang, K., Cheng, H., Hng, H., Ma, J., Mi, J., Zhao, X., . . . Zhang, Y. (2009). Synthesis and thermoelectric properties of double-filled skutterudites Ce y Yb 0.5− y Fe 1.5 Co 2.5 Sb 12. *Journal of Alloys and Compounds, 467*(1), 528-532.

Zakeri, M., Allahkarami, M., Kavei, G., Khanmohammadian, A., & Rahimipour, M. (2009). Synthesis of nanocrystalline Bi 2 Te 3 via mechanical alloying. *journal of materials processing technology, 209*(1), 96-101.

Zhang, L., Grytsiv, A., Kerber, M., Rogl, P., Bauer, E., & Zehetbauer, M. (2010). Thermoelectric performance of mischmetal skutterudites Mm y Fe 4− x Co x Sb 12 at elevated temperatures. *Journal of Alloys and Compounds, 490*(1), 19-25.

Zhang, L., Grytsiv, A., Kerber, M., Rogl, P., Bauer, E., Zehetbauer, M., . . . Nauer, G. (2009). MmFe 4 Sb 12-and CoSb 3-based nano-skutterudites prepared by ball milling: Kinetics of formation and transport properties. *Journal of Alloys and Compounds, 481*(1), 106-115.

Zhang, L., Grytsiv, A., Kerber, M., Rogl, P., Bauer, E., Zehetbauer, M. J., . . . Nauer, G. E. (2009). MmFe4Sb12- and CoSb3-based nano-skutterudites prepared by ball milling: Kinetics of formation and transport properties. *Journal of Alloys and Compounds, 481*(1–2), 106-115. doi: http://dx.doi.org/10.1016/j.jallcom.2009.03.109

Zhang, L., & Sakamoto, J. (2013). The microstructural stability and thermoelectric properties of Mm 0.9 Fe 3.5 Co 0.5 Sb 12-based skutterudites. *Materials chemistry and physics, 138*(2), 601-607.

Zhao, D., Geng, H., & Teng, X. (2012). Synthesis and thermoelectric properties of Ga x Co 4 Sb 11.7 Te 0.3 skutterudites. *Intermetallics, 26*, 31-35.

Zhou, C., Morelli, D., Zhou, X., Wang, G., & Uher, C. (2011). Thermoelectric properties of P-type Yb-filled skutterudite YbxFeyCo4-ySb12. *Intermetallics, 19*(10), 1390-1393.

List of Publications and Papers Presented

Raihan, O., Said, S. M., Sabri, M. F. M., Rozali, S., Long, B. D., Kimura, K., ... & Bashir, M. B. A. (2018). Parametric analysis of ball milling condition on thermoelectric performance of Bi0. 6FeCo3Sb12 skutterudite. *Materials Research Express*, *5*(10), 105008.